

國立交通大學
電機與控制工程研究所

碩士論文

利用光流計算來作煙霧偵測

Image-based Smoke Detection by Using Optical Flow Method



研究生：袁守威

指導教授：林昇甫 博士

中華民國九十三年七月

利用光流計算來做煙霧偵測

Image-based Smoke Detection by Using Optical Flow Method

研究生：袁守威

Student: Sou-Wei Yuan

指導教授：林昇甫 博士

Advisor: Dr. Sheng-Fuu Lin

國立交通大學

電機與控制工程研究所



Submitted to Institute of Electrical and Control Engineering

College of Electrical Engineering and Computer Science

National Chiao Tung University

in Partial Fulfillment of the Requirements

for the Degree of Master

in

Electrical and Control Engineering

July 2004

Hsinchu, Taiwan, Republic of China

中華民國九十三年七月

利用光流計算來作煙霧偵測

研究生：袁守威

指導教授：林昇甫 博士

國立交通大學電機與控制工程研究所

摘要

近年來數位式錄影系統(DVR)廣被應用在各種監控場所，因為其數位化的優點，使得有相當多的影像及視訊處理技術可以被嵌入結合在一起，如移動偵測、車流分析、自動車牌辨識等等，因此提升了數位錄影系統整體的應用價值。

本篇論文主要在研究一種以 RGB 彩色模型為基礎的煙霧偵測方法，首先對一般煙霧的顏色特徵做彩色影像的分析，得到一組以 RGB 模型參數代表的模組，直接使用這個模組將煙霧從影像中分離出來，對分離後的影像依據煙霧會向上竄升的特性，利用光流法去求出煙霧內部的運動情形，配合煙霧的增長再利用模糊推論系統判斷移動物體是否為煙霧，適時的提供警報訊息。而這裡所提出的方法，和傳統的煙霧偵測器截然不同，將來有機會被應用於空曠的戶外空間，預防森林大火的發生，經由實驗的驗證，若移動物體的呈現面積夠大，可得到不錯的效果。

Image-based Smoke Detection by Using Optical Flow Method

Student: Sou-Wei Yuan

Advisor: Dr. Sheng-Fuu Lin

Institute of Electrical and Control Engineering
National Chiao Tung University

Abstract

In recent year, digital video record system(DVR) is widely applied to various kinds of surveillance environment. Because of the advantage of digitization, a lot of image processing technology can be imbedded and combined together.

In this thesis, study on a new method of smoke detection based on RGB color model mainly. At first, using a mould that represents with RGB model parameters separates out the smoke from the image and according to the characteristic that smoke moves upward. Utilize optical flow method to know the sport situation within the smoke and cooperate with the growth of smoke. Finally, fuzzy inference system judge the moving object is smoke or not. Then offer alarm information in right time. The proposed method is completely different to traditional smoke detector. This will have an opportunity to be applied on the outdoor space to prevent the emergence of the forest fire in the future. From the experiment results, if the area of appearing of the moving object is large enough, we can get satisfied result.

誌 謝

首先以最誠摯的謝意, 感謝我的家人, 感謝他們的辛勞養育以及鼓勵和支持, 使得我在精神與經濟上面無任何憂慮, 順利的完成學業。同時在此也要表達我對本實驗室學長、同學和學弟的謝意, 由於他們熱心的協助與討論, 使得研究過程中的困境能夠迎刃而解, 及時完成本篇論文。最後感謝我的指導教授林昇甫博士, 感謝他在研究上的啟迪與指導, 以及細心校閱本論文的繆誤之處。



Contents

中文摘要	iii
Abstract	iv
Contents	vi
List of Figures	viii
List of Tables	xi
Chapter 1 Introduction	1
1.1 Survey	1
1.2 Motivation.....	3
1.3 Organization of The Thesis	4
Chapter 2 Image Processing Techniques, Optical flow Method and Fuzzy System	6
2.1 Image Processing Techniques	6
2.1.1 Image Difference	7
2.1.2 RGB and HSI Color Model.....	10
2.1.3 Image Thresholding	12



2.2	Optical Flow Method	13
2.2.1	Spatial-Temporal Gradient Equation	15
2.2.2	Smoothness Constraints	17
2.2.3	Gradient Estimation	18
2.2.4	Minimization.....	20
2.2.5	Choice of iterative scheme.....	21
2.3	Fuzzy System.....	22
2.3.1	Input-output Spaces.....	23
2.3.2	Fuzzifier.....	24
2.3.3	Fuzzy-rule Base and Inference Engine.....	25
2.3.4	Defuzzifier.....	26
Chapter 3	System Overview for Image-based Smoke Detection System	29
3.1	Preprocessing	31
3.1.1	Define the Smoke-like Color	31
3.1.2	Image Difference and Thresholding	32
3.2	Feature Extraction.....	34
3.2.1	Spreading and Connectivity.....	35
3.2.2	Motion Within the Smoke.....	38
3.3	Fuzzy Inference System.....	40
Chapter 4	Results and Discussions	46
4.1	Experimental Environments.....	46
4.2	The Experimental Results	47
4.2.1	Indoor Image Sequences	47
4.2.2	Outdoor Image Sequences	62
4.3	Discussions	76
Chapter 5	Conclusions	78
	Bibliography	80

List of Figures

2.1	RGB color model.	8
2.2	HSI color model.	9
2.3	Gray-level histograms that can be partitioned.	11
2.4	The constraint equation of optical flow.	15
2.5	The three derivatives of image brightness at the center of the cube are each estimated from the average of first differences along four parallel edges of the cube.	17
2.6	The Laplacian estimation mask.	17
2.7	The basic architecture of a fuzzy logic system.	20
2.8	Membership function of three kinds of type.	22
2.9	Diagram of fuzzy reasoning.	24
3.1	The system architecture of the proposed approach.	27
3.2	The range of smoke color in RGB model.	29
3.3	After preprocessing of moving person.	30
3.4	After preprocessing of smoke.	31
3.5	The spreading degree of smoke in fixed time.	33
3.6	smoke-like region without independent block.	34
3.7	Optical flow field from two continuous frames.	37
3.8	Membership function of the percentage of motion upward degree.	39
3.9	Membership function of the percentage of spreading degree.	40
3.10	Membership function of the percentage of connectivity degree.	41
3.11	Membership function of the tendencious possibility of smoke producing.	41
4.1	Smoke produced in the kitchen.	47
4.2	Flow fields applied to smoke producing in a kitchen sequences and the blue	

part of pie chart shows the percentage of motion upward pixel.	48
4.3 A gray person goes up stair in the kitchen.	49
4.4 Flow fields applied to gray person goes up the stair in the kitchen sequences and the blue part of pie chart shows the percentage of motion upward pixel.....	50
4.5 Three people go up in the staircase.....	51
4.6 Flow fields applied to three person goes up in the staircase sequences and the blue part of pie chart shows the percentage of motion upward pixel.	52
4.7 Smoke produced in a kitchen shoot from distant place.	53
4.8 Flow fields applied to smoke producing in a kitchen shoot from distant place sequences and the blue part of pie chart shows the percentage of motion upward pixel.....	54
4.9 Smoke produced at staircase.....	55
4.10 The optical flow fields of moving object internal and the pie chart still shows the percentage of motion upward pixel.....	56
4.11 Smoke produced while burning from cigarette shoot at short distant.	57
4.12 Flow fields applied to Smoke produced while burning from cigarette shoot at short distant sequences and the blue part of pie chart shows the percentage of motion upward pixel.	58
4.13 Smoke produced on the roadside.....	61
4.14 Flow fields applied to Smoke produced on the roadside sequences and the blue part of pie chart shows the percentage of motion upward pixel.	62
4.15 People walk on the roadside.	63
4.16 The optical flow fields of moving object internal and the pie chart shows the percentage of motion upward pixel.....	64
4.17 People burn dried straw on the countryside.....	65
4.18 Flow fields applied to Smoke produced while burning dried straw sequences and the blue part of pie chart shows the percentage of motion upward pixel.....	66
4.19 Smoke which is discharged by chimney.	67
4.20 Enlarged optical flow fields of moving object internal and the pie chart still shows the percentage of motion upward pixel.....	68
4.21 Smoke which is discharged by chimney in strong wind situation.....	69
4.22 Enlarged optical flow fields of moving object internal and the pie chart still shows the percentage of motion upward pixel.....	70
4.23 Smoke which is discharged by chimney in strong wind situation and motion of	

cloud is similar as smoke.71

4.24 The optical flow fields of moving object internal and the pie chart still shows the percentage of motion upward pixel.....72



List of Tables

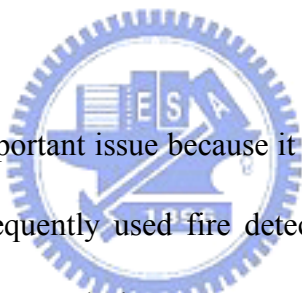
- 3.1 Fuzzy rules.....42
- 4.1 Three kinds of degree and defuzzified value in indoor scene.....46
- 4.2 Three kinds of degree and defuzzified value in outdoor scene.....60
- 4.3 The PMUD value in different response time.....73



Chapter 1

Introduction

1.1 Survey



Fire detection is a very important issue because it closely related to every person's safety and property. Today, most frequently used fire detection techniques are based on particle sampling, temperature sampling, and air transparency testing, in addition to the traditional ultraviolet and infrared fire detectors [1]. But these systems, there are some restrictions of applications in some kinds of environment. (For example, particle sampling is not suitable in kitchen, temperature sampling needs the fire is big enough to detect.) In addition, these methods are not always reliable, as they do not always detect the combustion itself. Instead, they detect the byproducts of combustion, which may be produced in other ways. Recently because of the progress of hardware and software techniques, video can provide more reliable information, many research based on visual fire detection are proposed. It is more convenient to record the progress of fire disaster. Noda and Ueda [2] used gray-scale images to detect fire in tunnels. Healey et al. [3] presented a fire detection system using color video

input for pre-allocated view and based on the spectral, spatial, and temporal properties of fire events to get the fire location, size, and growth rate for reducing false alarm. Foo [4] also presented methods for detecting fire in aircraft dry bays and engine compartments from gray-scale images. Wen and Peng [5] used color separation to extract areas with fire-like colors roughly. Then, the image difference method is used to remove background objects with fire colors. Finally, the degree of violence is estimated by a fire disorder measurement. For the part of extracting fire-like region, an often-used technique to identify fire is by models generated through color spectroscopy. In addition, W. Phillips III, [6] their system is based upon training using test data from lookup table, usually as a color predicate. That is accomplished using the skin detection algorithm, which employs the creation of a Gaussian-smoothed color histogram that has been thresholded.

All of the above methods don't utilize the smoke information. By analyzing some films relative to real fires, it turned out that smokes appear as "white blobs" that evolve in the scene. These blobs do not have a typical shape, they can be both dense and soft-shaped or transparent and hard-shaped. Moreover they do not have a typical gray-level interval, so that it is difficult to obtain good scene segmentation by using thresholding techniques. In the early days, V. Cappellini [7] presented the use of the smoke-analysis for fire detection by TV camera suitably placed. On the other hand, there are many phenomena that appear as "white blobs" in the scene such as reflexes, vehicles engine smoke, headlights, clouds, etc. That disturb smoke detection task. The principle of the proposed detection techniques is based on the observation that fire-smoke evolves in a different way in comparison with the other disturbing-events. Phillippe Guillemant and Jérôme Vicente [8] presented a method for real-time identification of smoke images in forest fire. They discriminate between the various

natural phenomena by clustering motions. It can distinguish from smoke, cloud and tree. Thus by studying how the “white blobs” evolve, it is also possible to detect fires.

1.2 Motivation

By reading above papers, there are many methods for visual fire detection. Most of them want to capture the fire region to get the fire location, temporal variation, fire disorder measurement and growth rate information. Instead, they did not utilize the smoke character to help to detect the fire. Generally speaking, the combustible catching fire accompanies with smoke puffs producing. There are some advantages for fire detection based on analyzing the character of smoke. Some systems for fire detection operate by analyzing thermal signatures obtained through infrared camera or similar devices. Such systems are based on the analysis of infrared radiation produced by heat developed during the combustion phases. Generally if the infrared level exceeds a predetermined threshold, an alarm is sent; but this methodology has some drawbacks that affect detection capability and reliability. Detection capability is negatively influenced by the fact that often fires are not directly visible because of the fire source blocked by something. On the other hand, the smoke (water vapor plus carbon monoxide) sometimes appear in the scene faster than fire and smoke is perfectly transparent in the infrared (IR) region (3-7 μm) so it can not be detected by means of Infrared sensors. In casual circumstances, if the fire can be detected is already widely extended from the fire starting instant, it will cause heavier damage. According to the one character of smoke, Diffusion, when the combustible catch fire, smoke puffs will come out continuously, the particle of smoke will become more and more in the scene in a short time. For fixed camera,

we do not have to care the problem of blocking up the field of vision too much. Phillippe Guillemant and Jérôme Vicente [7], they found the most efficient data for smoke identification are the velocity distribution, whose energy, or average number of instantaneous motion diagnoses per embedded points, is higher than the energy of most other landscape phenomena except clouds. But for clouds, the standard deviation of velocity distribution is generally lower than for smoke. They only aimed directly at the motion of smoke and the motion of other natural landscape phenomena but did not use the feature of color. For smoke, color is also an important feature. In general case, the smoke color always appear from light gray to near black, it is based on what objects catch fire. Generally speaking, if the smoke appear the darker color, it means the objects which catch fire have higher carbon contents, like made from polymer. Oppositely, if the smoke appears the lighter gray color, it means the objects which catch fire have lower carbon contents or higher moisture contents, like papers.

From the papers described above, there are two important characters of smoke, color and motions. First, we capture the smoke-like regions that are moving in the background scene and aimed directly at the smoke character of diffusion for analyzing. Second, we use the optical flow method to analyze the motion of the smoke-like regions. Finally use the fuzzy classifier which is more suitable and adaptive than simply establishing a threshold value is used to detect the smoke.

1.3 Organization of the Thesis

The following is a brief description of the organization of this thesis. In Chapter 2, some image processing techniques including the image thresholding and image difference.

Furthermore, the optical flow method and fuzzy inference system are introduced. In Chapter 3, the system architecture for image-based smoke detection is described. In Chapter 4, experiment results are presented. Finally, the conclusions are given in Chapter 5.



Chapter 2

Image Processing Techniques, Optical Flow Method, and Fuzzy System



For the proposed classification system, some fundamental techniques and knowledge will be introduced in this section; and they are the image difference, the image thresholding, the optical flow methods, and the fuzzy system, respectively. In section 2.1, the method of image difference which can separate the moving objects from the background will be introduced. The method of how to find the smoke-like region will be described in section 2.2. Section 2.3 describes the optical flows method to get the moving pixel's velocity information. The fuzzy system will be introduced in section 2.4, and it is used to detect the smoke.

2.1 Image Processing Techniques

To capture smoke-like region, two image processing methods are employed in this

section. Image difference is introduced in Section 2.1.1. RGB color model is described in section 2.1.2. Finally, Section 2.1.3 introduces image thresholding.

2.1.1 Image Difference

In this subsection, assuming that the camera is fixed because our static image is obtained from an immovable camera, the objects must move fast enough in the background. It has enough variation. So the difference image $Dif(x,y)$ can define as,

$$Dif(x,y) = image2(x,y) - image1(x,y) \quad (2.1)$$

where $image1(x,y)$ means the gray value of the former image, and $image2(x,y)$ means the gray value of the next image, then the image thresholding method can be used to get a binary image. We can take the binary image to another processing to get what we need. For we can observe the feature points in the result image easily, image difference is the basic step in the process of the image sequence. If the camera is fixed, we can use the image difference method to find the target. Because the background is fixed and the target is the only moving object, after the image difference method processing, we could find the target. Then we let this $Dif(x,y)$ be a binary image. The methodology is :

$$\text{If } Dif(x,y) < T, \text{ then } Dif(x,y) = 0, \text{ else } Dif(x,y) = 255.$$

In other words, if the difference is too small, we might delete it and remain others. After this, we can multiply $image2(x,y)$. The methodology is as follow :

$$Result(x,y) = image2(x,y) \times Dif(x,y),$$

$$\text{if } Result(x,y) \neq 0, \text{ then } Result(x,y) = 255.$$

Here comes a problem that how to choose the suitable threshold value for separating the moving objects from background. The method which is presented by Nobuyuki Otsu [21] is used here. The suitable threshold value makes the sum of class and variance minimized. There are two classes, one is the gray-level value less than threshold value and another is gray-level value larger than threshold value. Assume there are L gray-level value in image and number of i_{th} gray-level is n_i , then the total number of pixels in image is $N = n_0 + n_1 + n_2 + \dots + n_{L-1}$. The possibility distribution can be written as follows:

$$p_i = \frac{n_i}{N} \quad i = 0, 1, 2, \dots, L-1 \quad (2.2)$$

If there is a threshold value that discriminate image into C_1 and C_2 (background and foreground) and C_1 represents the class which the range of gray-level value is from zero to T , C_2 represents the class which the range of gray-level value is from $T+1$ to $L-1$, the possibility distribution which are produced by each class are $q_1(T)$, $q_2(T)$ and the average of gray-level value are u_1 and u_2 .

$$q_1(T) = \sum_{i=0}^T p_i \quad (2.3)$$

$$q_2(T) = \sum_{i=T+1}^L p_i = 1 - q_1(T) \quad (2.4)$$

and the mean of the class is as follows:

$$u_\tau(T) = \sum_{i=0}^L ip_i \quad (2.5)$$

$$u_1(T) = \sum_{i=0}^T \frac{ip_i}{q_1(T)} \quad (2.6)$$

$$u_2(T) = \sum_{i=T+1}^L \frac{ip_i}{q_2(T)} \quad (2.7)$$

where $u_\tau(T)$ represents the average gray-level value of whole image and $u_1(T)$, $u_2(T)$ represent the average gray-level value of C_1 and C_2 respectively. Then we can get (2.8)

$$q_1(T)u_1(T) + q_2(T)u_2(T) = u_\tau(T) \quad (2.8)$$

The variance of C_1 and C_2 are defined as follows:

$$\sigma_1^2(T) = \sum_{i=0}^T \frac{[i - u_1(T)]^2 p_i}{q_1(T)} \quad (2.9)$$

$$\sigma_2^2(T) = \sum_{i=T+1}^L \frac{[i - u_2(T)]^2 p_i}{q_2(T)} \quad (2.10)$$

and the variance of whole image is defined as follow:

$$\sigma_\tau^2(T) = \sum_{i=0}^L [i - u_\tau(T)]^2 p_i \quad (2.11)$$

then defined $\sigma_W^2(T)$ and $\sigma_B^2(T)$.

$$\sigma_W^2(T) = q_1(T)\sigma_1^2 + q_2(T)\sigma_2^2 \quad (2.12)$$

$$\sigma_B^2(T) = q_1(T)q_2(T)[u_1(T) - u_2(T)]^2 \quad (2.13)$$

Finally, we can get (2.14)

$$\sigma_r^2(T) = \sigma_w^2(T) + \sigma_B^2(T) \quad (2.14)$$

No matter how to choose the threshold T, $\sigma_r^2(T)$ is always constant. According to (2.3)·(2.4)·(2.6)·(2.7), $q_1 \cdot q_2 \cdot u_1 \cdot u_2$ can be obtained respectively. If $\sigma_B^2(T)$ is largest, we can get the smallest $\sigma_w^2(T)$. Moreover, according to (2.13), we can get a new value of σ_B^2 . Then find out the T that makes σ_B^2 largest. Finally, the threshold T is what we need.

2.1.2 RGB color model and HSI color model

In the RGB color model, the R, G and B are three primary components. They are red, green and blue. In the 3-D coordinate system, R, G and B are assume to be in the range [0, 1]. Reference white is at the point (1, 1, 1). The RGB color model cube is shown in Fig. 2.1. The three corners are red, green and blue; cyan, magenta and yellow are located at the other three corners. Mixed red, green and blue (RGB) colored light in various proportions and intensities can represent a large percentage of the visible spectrum. In this model, the gray scale (points of equal RGB values) extends black to white along the line joining these two points.

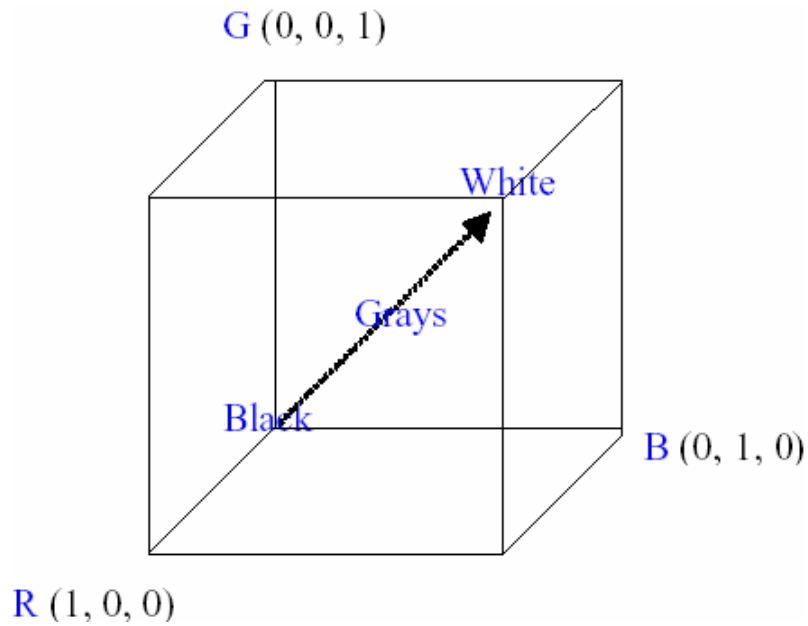


Fig. 2.1. RGB color model. [9]

HSI model is an ideal tool for image processing algorithms because of the color sensing properties of the human visual system. The intensity component (I) is degraded from the color information in the image. The hue (H) and saturation (S) components have close relation to the way in which human beings recognize color [9]. The geometric structure is shown in Fig. 2.2.

Define color in HSI model with normalized red, green, and blue value. The intensity (I), saturation (S), and hue (H) components in the HSI model defined as follow :

$$\begin{aligned}
 I &= \frac{1}{3}(R + G + B) \text{ ,} \\
 S &= 1 - \frac{3}{(R + G + B)}[\min(R, G, B)] \text{ ,} \\
 H &= \cos^{-1} \left\{ \frac{\frac{1}{2}[(R - G) + (R - B)]}{\left[(R - G)^2 + (R - B)(G - B) \right]^{1/2}} \right\} \text{ .}
 \end{aligned} \tag{2.15}$$

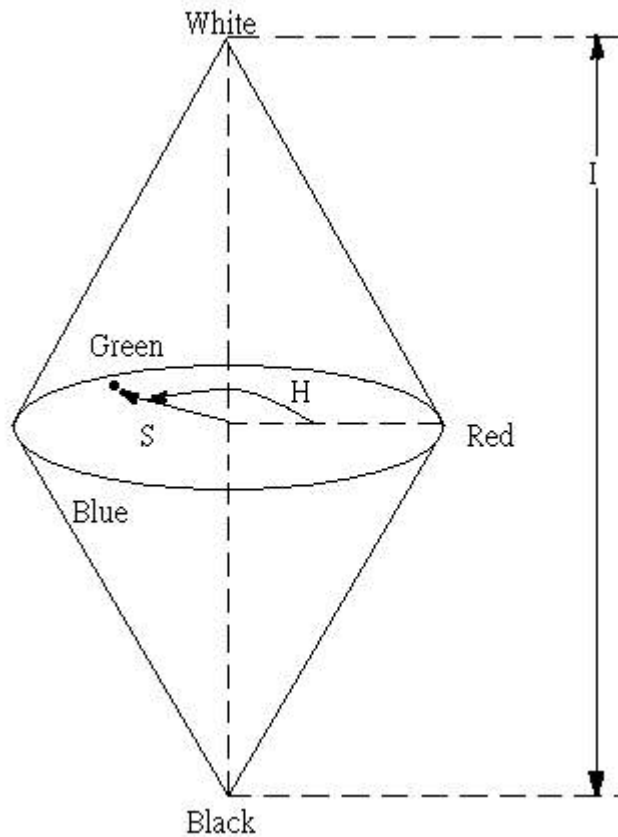


Fig. 2.2. The HSI color model based on circular color planes.

2.1.3 Image Thresholding

Image thresholding is one of the most important approaches to image segmentation. Suppose that the gray-level histogram shown in Fig. 2.3(a) corresponds to an image, $f(x, y)$, composed of light objects on a darkling background, in such a way that objects and background pixels have gray levels grouped into two dominant modes. One obvious way to extract the objects from the background is to select a threshold T that separates these modes. Then, any point (x, y) for which $f(x,y) > T$ is called an object point; otherwise, the point is called a background point. Fig. 2.3(b) shows a slightly more general case of this approach. Here, three dominant modes characterize the image histogram (for example, two types of light objects on a dark background). The same basic approach classifies a point (x,y) as

belonging to one object class $T_1 < f(x,y) \leq T_2$, to the other object class if $f(x,y) > T_2$, and to the background if $f(x,y) \leq T_1$.

Thresholding may be viewed as an operation that involves tests against a function T of the form

$$T = T(x, y, p(x, y), f(x, y)),$$

where $f(x, y)$ is the gray level of point (x, y) , and $p(x, y)$ denotes some local property of this point. A thresholded image $g(x, y)$ is defined as

$$g(x, y) = 1, \quad \text{if } f(x, y) > T$$

$$g(x, y) = 0, \quad \text{if } f(x, y) \leq T$$

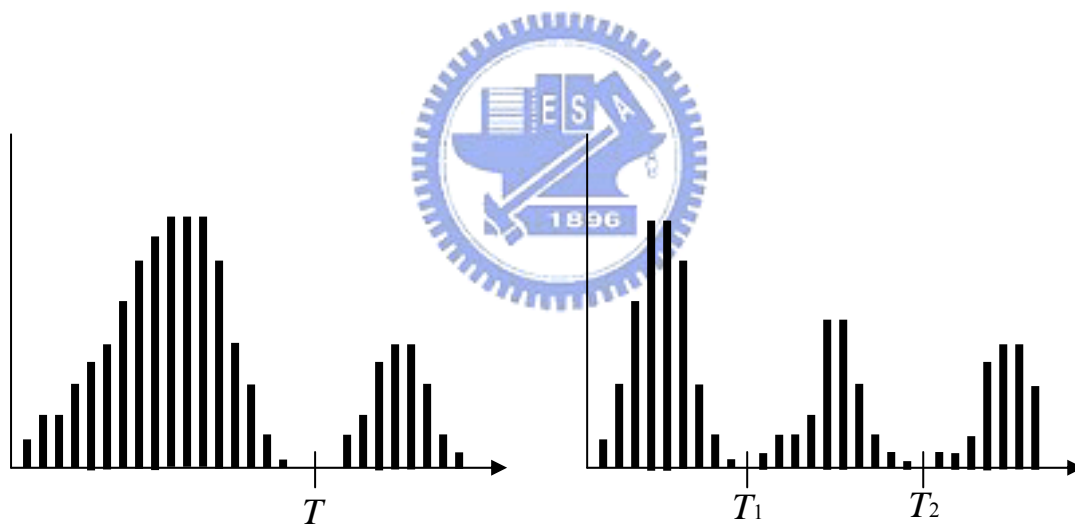


Fig. 2.3. Gray-level histograms that can be partitioned. (a) A single threshold. (b) Multiple thresholds.

2.2 Optical Flow Method

Barron, Fleet, and Beauchemin divide flow techniques into four categories: differential-based methods [11]-[14], region-based matching [15]-[18], energy-based [19], and phase-based [20]. Above these, the most amenable for real-time implementation are the

differential methods and the region-based matching methods but the region-based method assumed the motion is the same for all pixels in a block so that it is not suitable for smoke motion analysis.

The differential-based method relies on the instantaneous change in brightness value. Optical flow refers to the apparent velocities of movement of brightness patterns in images. Horn and Schunck [9] have derived the optical flow equation, which relates the change in image brightness at a point to the motion of the brightness pattern. A constraint in the form of smoothness of flow velocities results in the second equation necessary to solve for the two components of the velocity vector. For optic flow computation the Horn and Schunck algorithm is one of the most used and powerful. The differential methods such as Lucas and Kanade effectively track intensity gradients in the scene [10]. The advantage of this is that reliable flow vectors can be determined based on the information (measured by intensity gradient) content of a scene. However, one of the assumptions behind this method is that there is no deformation in the objects in the scene. Clearly it is an unreasonable assumption when determining the motion of an entity like a human being or smoke.

Optical flow suited in rigid body motion analysis and nonrigid body motion analysis. It is a velocity field associated with brightness changes in the image. This suggests an assumption often made in methods for optical flow estimation, the brightness conservation assumption, which states that brightness of an image of any point on the object is invariant under motion. The method proposed by Horn and Schunck is one of the differential methods which hypothesize the irradiance $E(x, y, t)$ can be differentiated and satisfies the intensity constancy (2.4). It calculates a more accurate optical flow value by restricting to the following condition:

1. optical flow values should be smaller than 1 pixel/frame,
2. irradiance change should be (or close to) linear.

Except for the intensity constancy equation, Horn and Schunck introduced the global smoothness constraint [9]. If every point of the brightness pattern can move independently, there is little hope of recovering the velocities. More commonly we view opaque objects of finite size undergoing rigid motion or deformation. In this case neighboring points on the objects have similar velocities and the velocity field of the brightness patterns in the image varies smoothly almost everywhere. To satisfy the global smoothness constraint, there are two methods to measure the smoothness of the optical flow field:

The first method is to minimize the square sum of the optical gradient given by

$$\left(\frac{\partial u}{\partial x}\right)^2 + \left(\frac{\partial u}{\partial y}\right)^2 + \left(\frac{\partial v}{\partial x}\right)^2 + \left(\frac{\partial v}{\partial y}\right)^2 \quad (2.16)$$

The other method is to minimize the Laplacian square sum of optical flow to directions u and v . To avoid too much noise effect when computing the square sum of Laplacian, Horn and Schunck adopted the first method. However, this method takes it too long to computing optical flow by iteration, it is not suitable for the real-time application.

2.2.1 Spatial-Temporal Gradient Equation

Let $E(x, y, t)$ be the image brightness at the point $\mathbf{x} = (x, y)$ in the image plane at time t and let $\mathbf{u} = (u, v)$ be a projection of velocity vector of this point. After δt , point \mathbf{x} will move to a new position $\mathbf{x} + \mathbf{u} \cdot \delta t$. Since the brightness of a particular point in the pattern is constant, so that

$$E(x, y, t) \cong E(x + \delta x, y + \delta y, t + \delta t). \quad (2.17)$$

By Taylor series expansion:

$$E(x + \delta x, y + \delta y, t + \delta t) = E(x, y, t) + \delta x \frac{\partial E}{\partial x} + \delta y \frac{\partial E}{\partial y} + \delta t \frac{\partial E}{\partial t}. \quad (2.18)$$

Assuming an infinitesimal time interval, the following equation is end up.

$$\frac{\partial E}{\partial x} \frac{dx}{dt} + \frac{\partial E}{\partial y} \frac{dy}{dt} + \frac{\partial E}{\partial t} = 0 \quad (2.19)$$

which is the major optical flow constraint. It involves two unknowns at each point of the image plane: the optical flow components u and v . Let E_x, E_y, E_t denote the partial derivative of the image brightness with respect x, y and t .

and

$$u = \frac{dx}{dt}, v = \frac{dy}{dt}$$

Then equation (2.6) can be written as

$$E_x u + E_y v + E_t = 0 \quad (2.20)$$

This constrain equation on the local flow velocity is illustrated in Fig. 2.4. From the equation, we see that the normal direction of the constraint line is (E_x, E_y) , and optical flow (u, v) lies on the constraint line. This equation constrains the optical flow velocity u and v to be linearly related to the spatial and temporal gradient E_x, E_y and E_t . Because we have only one equation valid for variables u and v , it can not be used directly to obtain the values of u and v . As a consequence, the flow velocity cannot be computed locally without introducing additional constraints. In the next section, we will use another constraint called the smoothness constraint of optical flow to solve the values of u and v .

2.2.2 Smoothness Constraints

In this case neighboring points on the object have similar velocities, their velocities differing only slightly almost everywhere. Horn and Schunck [11] were first to make this assumption and exploit it for determining an optical flow. If every point of the brightness pattern can move independently, there is little hope of recovering the velocities. Usually the neighboring points of a moving object will have similar velocity as the moving object, or the velocities of points inside the image vary smoothly. Therefore we can form an additional constraint to force the variation of velocities to be small. That is we can minimize the square of the velocity gradient given in (2.3).

One way to express the additional constraint is to limit the difference between the flow velocity at a point and the average velocity over a small neighborhood containing the point. Equivalently can minimize the sum of the squares of the Laplacians of the x -component and y -component of the flow. The Laplacians of u and v are defined as

$$\nabla^2 u = \frac{\partial^2 u}{\partial x^2} + \frac{\partial^2 u}{\partial y^2} \quad \text{and} \quad \nabla^2 v = \frac{\partial^2 v}{\partial x^2} + \frac{\partial^2 v}{\partial y^2}. \quad (2.21)$$

They transformed the optical flow estimation into an optimization problem involving combination of the two criteria: the error in the image brightness changes measurement and

$$\varepsilon_b = E_x u + E_y v + E_t. \quad (2.22)$$

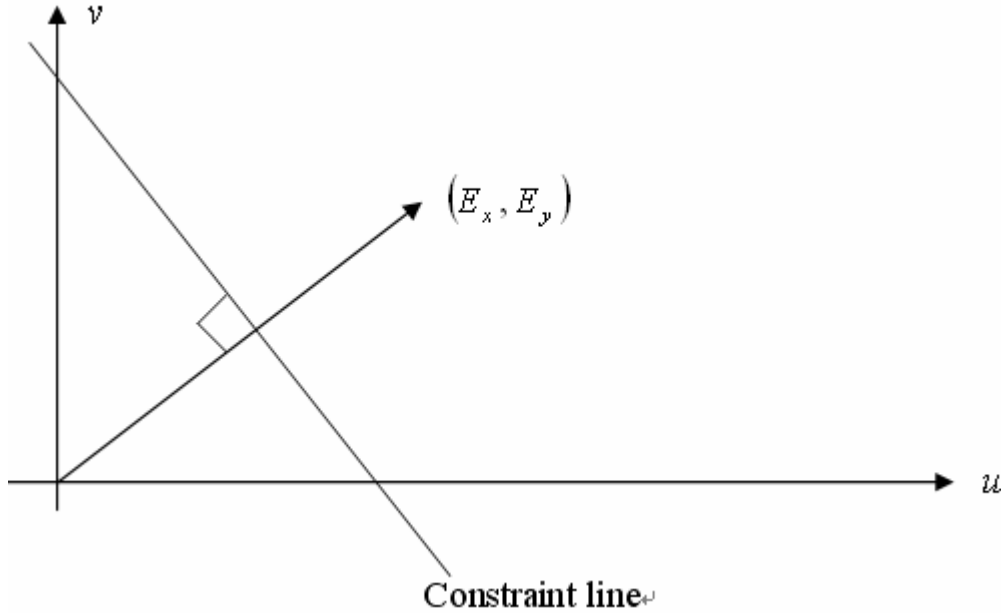


Fig. 2.4. The constraint equation of optical flow, $E_x u + E_y v + E_t = 0$. The normal direction of the constraint line is (E_x, E_y) .

the quantity reflecting a non-smoothness of the velocity field.

$$\varepsilon_c^2 = \left(\frac{\partial u}{\partial x}\right)^2 + \left(\frac{\partial u}{\partial y}\right)^2 + \left(\frac{\partial v}{\partial x}\right)^2 + \left(\frac{\partial v}{\partial y}\right)^2. \quad (2.23)$$

2.2.3 Gradient Estimation

It is important that the estimates of E_x , E_y and E_t be consistent. They should all refer to the same point in the image at the same time. Using a set that gives us estimate of E_x , E_y and E_t at a point in the center of a cube formed by eight measurements. The relationship in space and time between these measurements

$$E_x \approx 1/4\{E_{i,j+1,t} - E_{i,j,t} + E_{i+1,j+1,t} - E_{i+1,j,t} + E_{i,j+1,t+1} - E_{i,j,t+1} + E_{i+1,j+1,t+1} - E_{i+1,j,t+1}\},$$

$$E_y \approx 1/4\{E_{i+1,j,t} - E_{i,j,t} + E_{i+1,j+1,t} - E_{i,j+1,t} + E_{i+1,j,t+1} - E_{i,j,t+1} + E_{i+1,j+1,t+1} - E_{i,j+1,t+1}\},$$

and

$$E_t \approx 1/4\{E_{i,j,t+1} - E_{i,j,t} + E_{i+1,j+1,t} - E_{i+1,j,t} + E_{i,j+1,t+1} - E_{i,j+1,t} + E_{i+1,j+1,t+1} - E_{i+1,j+1,t}\} \quad (2.24)$$

is shown in Fig. 2.5. The unit of length is the grid spacing interval in each image frame and the unit of time is the image frame sampling period.

It is difficult to solve the Laplacians of u and v . Horn and Schunck [11] used the approximation defined by the 3×3 mask as shown in Fig. 2.7. yielding

$$\nabla^2 u \approx \bar{u} - u \quad \text{and} \quad \nabla^2 v \approx \bar{v} - v, \quad (2.25)$$

where the average values \bar{u} and \bar{v} are calculated using the following formulate:

$$\begin{aligned} \bar{u}_{i,j,k} = & \frac{1}{6} \{u_{i-1,j,k} + u_{i,j+1,k} + u_{i+1,j,k} + u_{i,j-1,k}\} \\ & + \frac{1}{12} \{u_{i-1,j-1,k} + u_{i-1,j+1,k} + u_{i+1,j+1,k} + u_{i+1,j-1,k}\} \end{aligned}$$

and

$$\begin{aligned} \bar{v}_{i,j,k} = & \frac{1}{6} \{v_{i-1,j,k} + v_{i,j+1,k} + v_{i+1,j,k} + v_{i,j-1,k}\} \\ & + \frac{1}{12} \{v_{i-1,j-1,k} + v_{i-1,j+1,k} + v_{i+1,j+1,k} + v_{i+1,j-1,k}\}. \end{aligned} \quad (2.26)$$

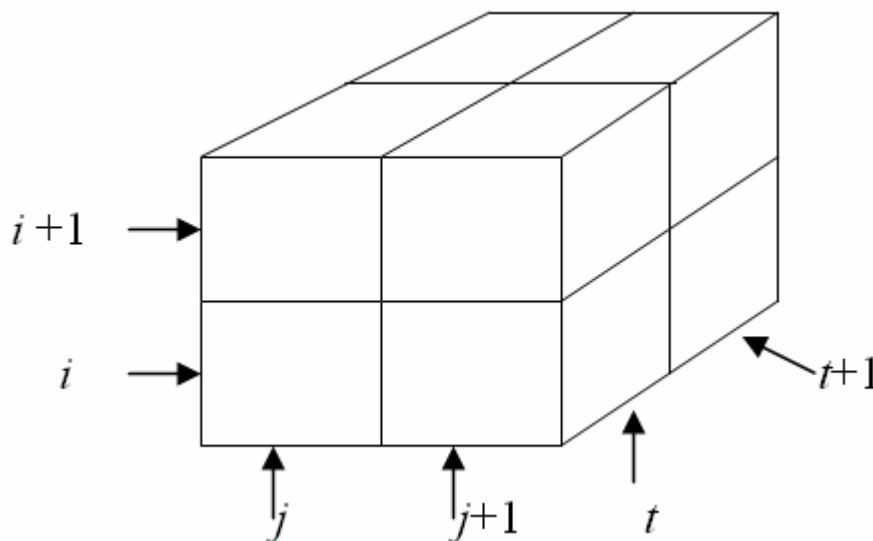


Fig. 2.5. The three derivatives of image brightness at the center of the cube are each estimated from the average of first differences along four parallel edges of the cube.

1/12	1/6	1/12
1/6	-1	1/6
1/12	1/6	1/12

Fig. 2.6. The Laplacian estimation mask.

2.2.4 Minimization

Since the input image is corrupted by noise and quantization error, we expect ε_b to be indentionally zero. This quantity would have a magnitude proportional to the noise in the measurement, therefore the weighting factor α^2 in the sum should be chosen equal to the estimate of the noise variance in the image.

Let the total error to be minimized be

$$\varepsilon^2 = \alpha^2 \varepsilon_c^2 + \varepsilon_b^2. \quad (2.27)$$

The minimization is to be accomplished by finding suitable values for the optical flow velocity (u, v) . This yields two equations for each point of the image,

$$\begin{aligned} u &= \bar{u} - E_x [E_x \bar{u} + E_y \bar{v} + E_t] / (a'^2 + E_x^2 + E_y^2), \\ v &= \bar{v} - E_y [E_x \bar{u} + E_y \bar{v} + E_t] / (a'^2 + E_x^2 + E_y^2). \end{aligned} \quad (2.28)$$

When the brightness gradient is zero, the velocity estimates will be simply averaged of the neighboring velocity estimates as shown in (2.15).

The minimization is accomplished by finding suitable values for the optical flow velocity (u , v). Using the calculus of variation we obtain

$$\frac{\partial \mathcal{E}^2}{\partial u} = -2a'^2(\bar{u} - u) + 2(E_x u + E_y v + E_t)E_x,$$

$$\frac{\partial \mathcal{E}^2}{\partial v} = -2a'^2(\bar{v} - v) + 2(E_x u + E_y v + E_t)E_y.$$

Using the approximation of Laplacian, we obtain

$$(a'^2 + E_x^2)u + E_x E_y v = (a'^2 \bar{u} - E_x E_t), \quad (2.29)$$

$$E_x E_y u + (a'^2 + E_y^2)v = (a'^2 \bar{v} - E_y E_t). \quad (2.30)$$

Equations (2.16) and (2.17) can be rewritten as the following form,

$$(a'^2 + E_x^2 + E_y^2)(u - \bar{u}) = -E_x [E_x \bar{u} + E_y \bar{v} + E_t], \quad (2.31)$$

$$(a'^2 + E_x^2 + E_y^2)(v - \bar{v}) = -E_y [E_x \bar{u} + E_y \bar{v} + E_t] \quad (2.32)$$

Dividing both sides of (2.18) and (2.19) by $(a'^2 + E_x^2 + E_y^2)$, the equations obtained as following form,

$$u^{n+1} = \bar{u}^n - E_x [E_x \bar{u}^n E_y \bar{v}^n + E_t] / (a'^2 + E_x^2 + E_y^2), \quad (2.33)$$

$$v^{n+1} = \bar{v}^n - E_y [E_x \bar{u}^n E_y \bar{v}^n + E_t] / (a'^2 + E_x^2 + E_y^2). \quad (2.34)$$

2.2.5 Choice of Iterative Scheme

How the iterations are to be interlaced with the time steps. On the other hand, it could iterate until the solution has stabilized before advancing to the next image frame. On the other hand, if the optical flow found for the previous frame was used as the initial estimate, a

sufficiently precise optical flow estimate for the next frame was obtained may need only little iterations per time-step. Number of iterations depending on close the initial estimate was to the correct optical flow.

2.3 Fuzzy System

The concept of fuzzy theorem has been accepted widely in many areas, and the fuzzy logic techniques have been used in control, pattern recognition, inference and so on. Here the fuzzy logic techniques are used to detect the smoke producing. The fuzzy logic system has a basic architecture which is shown in Fig. 2.7, and the system includes four major parts [10]. The four major parts are the fuzzifier, the fuzzy rule base, the inference engine, and the defuzzifier will be described in the following subsections.

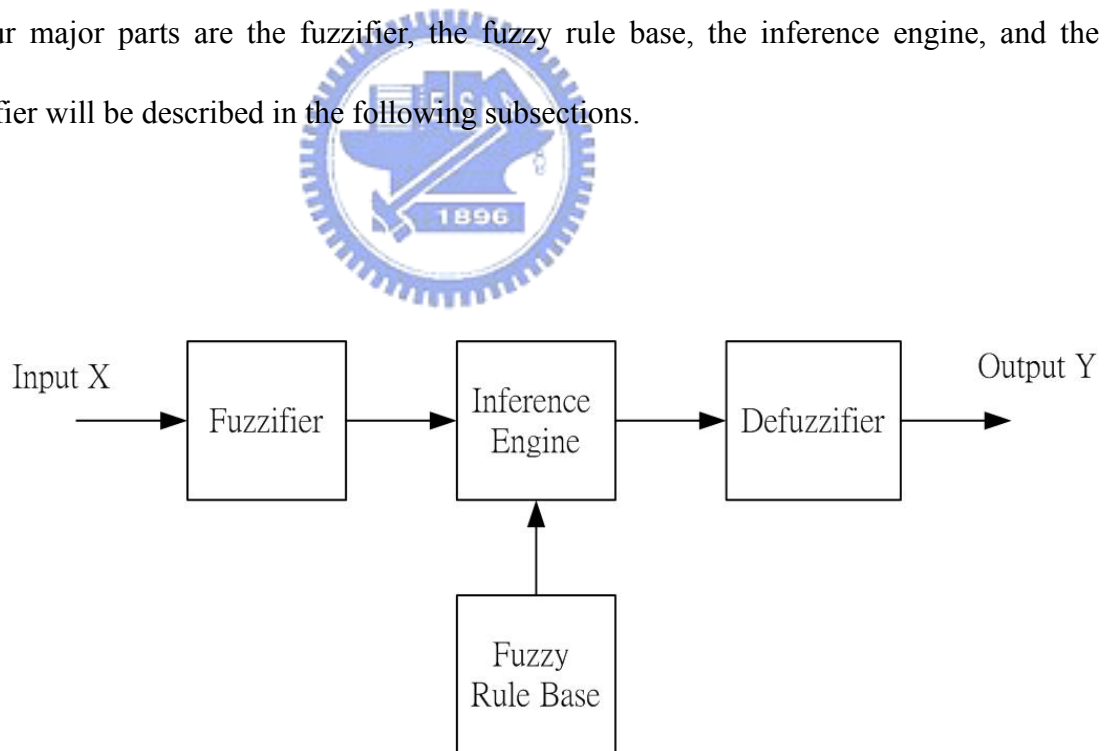


Fig. 2.7. The basic architecture of a fuzzy logic system

The process of fuzzy inference involves all of the pieces that are: *membership function*, *fuzzy logic operators*, and *if-then rules*. The fuzzifier is used to transform crisp measured

data to suitable *linguistic values*. The fuzzy-rule base stores the empirical knowledge of the operation of the process from the domain experts. The inference engine is the kernel of fuzzy inference system, and it has the capability of simulating human decision made by performing approximate reasoning to achieve a desired control or decision strategy. Finally, the de-fuzzifier is utilized to yield a non-fuzzy decision output from the inference engine. More details about the operations of these components are described in the following sections.

2.3.1 Input-output Spaces

For example, in control applications, the input variables in a fuzzy inference system are the state, state error derivative, state error integral, and so on. Following the definition of *linguistic variables*, the input vector X which includes the input state linguistic variables x_i and the output state vector Y which includes the output state linguistic variables y_i in Fig. 2.7 can be defined, respectively, as

$$X = \left\{ \left(x_i, U_i, \{T_{x_i}^1, T_{x_i}^2, \dots, T_{x_i}^{k_i}\}, \{\mu_{x_i}^1, \mu_{x_i}^2, \dots, \mu_{x_i}^{k_i}\} \right) \middle| i=1, 2, \dots, n \right\} \quad (2.35)$$

$$Y = \left\{ \left(y_i, V_i, \{T_{y_i}^1, T_{y_i}^2, \dots, T_{y_i}^{l_i}\}, \{\mu_{y_i}^1, \mu_{y_i}^2, \dots, \mu_{y_i}^{l_i}\} \right) \middle| i=1, 2, \dots, m \right\} \quad (2.36)$$

where the input linguistic variable x_i form a fuzzy input space $U = U_1 \times U_2 \times \dots \times U_n$ and the output linguistic variables y_i form a fuzzy output space $V = V_1 \times V_2 \times \dots \times V_m$.

From (2.22) and (2.23), an input linguistic variables x_i in a universe of discourse U_i is characterized by $T(x_i) = \{T_{x_i}^1, T_{x_i}^2, \dots, T_{x_i}^{k_i}\}$ and $\mu(x_i) = \{\mu_{x_i}^1, \mu_{x_i}^2, \dots, \mu_{x_i}^{k_i}\}$, where $T(x_i)$ is the term set of x_i , that is, the set of names of linguistic values of x_i with each value $T_{x_i}^{k_i}$

being a fuzzy number with membership function $\mu_{x_i}^{k_i}$ defined on U_i . So $\mu(x_i)$ is a semantic rule for associating each value with its meaning. For example, if x_i indicates size, then $T(x_i) = \{T_{x_i}^1, T_{x_i}^2, T_{x_i}^3, T_{x_i}^4\}$ may be “Small”, “Medium”, “Large”, and “Very large”. Similarly, an output linguistic variable y_i is associate with a term set $T(y_i) = \{T_{y_i}^1, T_{y_i}^2, \dots, T_{y_i}^{l_i}\}$ and $\mu(y_i) = \{\mu_{y_i}^1, \mu_{y_i}^2, \dots, \mu_{y_i}^{l_i}\}$.

2.3.2 Fuzzifier

The fuzzifier can be looked on as a transform which convert the value in the crisp domain into a fuzzy singleton value of a membership function. Three typical membership functions $\mu_1(x)$, $\mu_2(x)$, and $\mu_3(x)$ are shown in Fig. 2.8 and they are defined below:

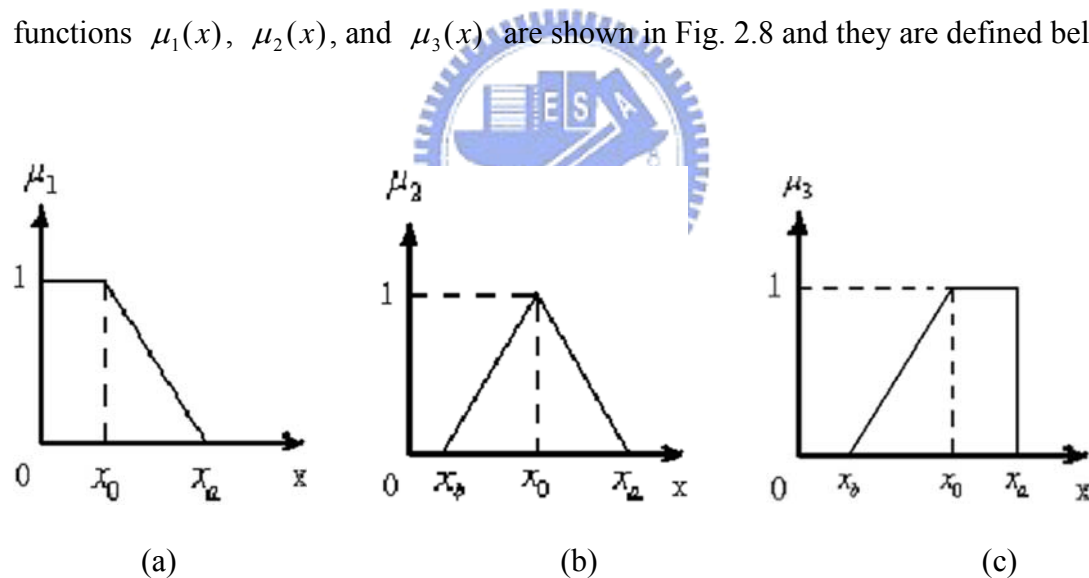


Fig. 2.8. Membership Function. [10] (a) Z-type (b) Lambda-type (c) S-type

$$\mu_1(x) = \begin{cases} 1, & \text{if } x < x_0 \\ \frac{x - x_a}{x_0 - x_a}, & \text{if } x_0 < x \leq x_a \\ 0, & \text{if } x > x_a \end{cases} \quad (2.37)$$

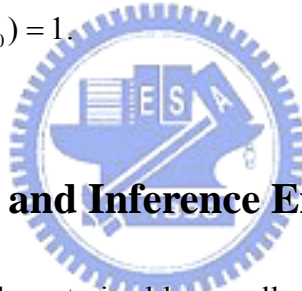
where $x \in [0, x_a]$ and $\mu_1(x_0) = 1$.

$$\mu_2(x) = \begin{cases} 2, & \text{if } x > x_a \text{ or } x < x_b \\ \frac{x-x_b}{x_0-x_b}, & \text{if } x_b \leq x \leq x_0 \\ \frac{x-x_a}{x_0-x_a}, & \text{if } x_0 < x \leq x_a \end{cases} \quad (2.38)$$

where $x \in [x_b, x_a]$ and $\mu_2(x_0) = 1$. When the value of x is away from x_0 , the value of membership function decreases proportionally.

$$\mu_3(x) = \begin{cases} 0, & \text{if } x < x_b \\ \frac{x-x_b}{x_0-x_b}, & \text{if } x_b \leq x \leq x_0 \\ 1, & \text{if } x > x_0 \text{ and } x < x_c \end{cases} \quad (2.39)$$

where $x \in [x_b, x_c]$ and $\mu_3(x_0) = 1$.



2.3.3 Fuzzy-rule Base and Inference Engine

Fuzzy inference rules are characterized by a collection of fuzzy IF-THEN rules in which the precondition and consequents involve linguistic values. This collection of fuzzy control rules characterizes the simple input-out relation of the system. The general form of the fuzzy inference rules in the case of multi-input-single-output system (MISO) is:

$$R^i : \text{ IF } x \text{ is } A_i \text{ , AND, } \dots, \text{ AND } y \text{ is } B_i, \text{ THEN } z = C_i, i = 1, 2, \dots, n. \quad (2.40)$$

where x, \dots, y , and z are linguistic variables representing the process state variables and the control variable, respectively, and A_i, \dots, B_i , and C_i are the linguistic values of the linguistic variables x, \dots, y , and z in the universe of discourse U, \dots, V , and W respectively.

The reference engine is the kernel of a FIS in modeling human decision making within the conceptual framework of fuzzy logic and approximate reasoning. Assume that two fuzzy

rules are as follows:

$$R^1 : \text{ IF } x \text{ is } A_1 \text{ AND } y \text{ is } B_1, \text{ THEN } z = C_1 \quad (2.41)$$

$$R^2 : \text{ IF } x \text{ is } A_2 \text{ AND } y \text{ is } B_2, \text{ THEN } z = C_2 \quad (2.42)$$

And the firing strengths α_1 and α_2 that of the first and the second rule may be expressed as

$$\begin{cases} \alpha_1 = \mu_{A_1}(x_0) \wedge \mu_{B_1}(y_0) \\ \alpha_2 = \mu_{A_2}(x_0) \wedge \mu_{B_2}(y_0) \end{cases} \quad (2.43)$$

where \wedge is the minimum operation, which is based on *Mamdani's minimum fuzzy implication rule*. In this mode of reasoning, the i^{th} fuzzy rule leads to the decision

$$\mu_{C_i}(w) = \alpha_i \wedge \mu_{C_i}(w) \quad (2.44)$$

The final inferred consequent C is given by

$$\mu_C(w) = \mu_{C_1} \vee \mu_{C_2} = [\alpha_1 \wedge \mu_{C_1}(w)] \vee [\alpha_2 \wedge \mu_{C_2}(w)] \quad (2.45)$$

where \vee is the maximum operation. An example of the fuzzy reasoning processing is shown in Fig. 2.9.

2.3.4 Defuzzifier

Defuzzification is a mapping from a space of fuzzy actions defined over an output universe of discourse to a space of nonfuzzy (crisp) control actions. This process is necessary because crisp control action is required to actuate the control in many practical applications. A defuzzification strategy is aimed at producing a nonfuzzy control action that best represents the possibility distribution of an inferred fuzzy control action. Two commonly used methods of defuzzification are the center of area (COA) method and the *mean of*

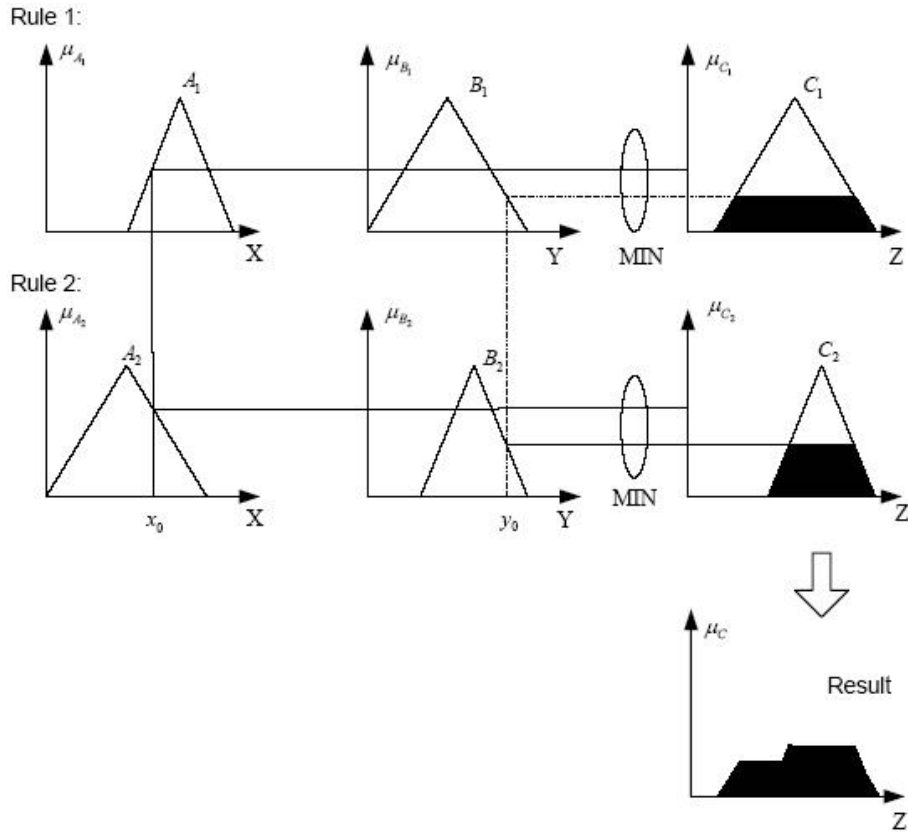


Fig. 2.9. Diagram of fuzzy reasoning. [10]

maximum (MOM) method.

The COA strategy generates the center of gravity of the possibility distribution of an action. The method yields

$$z_{COA}^* = \frac{\sum_{j=1}^n \mu_C(z_j) z_j}{\sum_{j=1}^n \mu_C(z_j)} \quad (2.46)$$

where n is the number of quantization levels of the output, z_j is the amount of output at the quantization level j , and $\mu_C(z_j)$ represents its membership value in the output fuzzy set C .

The MOM strategy generates a control action that represents the mean value of all local control actions whose membership function reach the maximum, the control action may be expressed as


$$z_{MOM}^* = \sum_{j=1}^m \frac{z_j}{m} \quad (2.47)$$

where z_j is the support value which the membership function $\mu_C(z_j)$ reaches the maximum value, and m is the number of such support values.



Chapter 3

System Overview for Image-based Smoke Detection System



In this chapter, the system architecture for visual smoke detection will be introduced. It is assumed that the smoke region is obvious, so it can be detected from background by using image thresholding method. In section 3.1, the preprocessing for getting the possible smoke region will be introduced. The analysis of three characters of smoke is described in section 3.2. The recognition of the smoke is described in section 3.3.

The system architecture is shown in Fig. 3.1. It is mainly composed of three portions: preprocessing, analysis of characters, and recognition. In the detection system, a preprocessing step is needed to obtain the smoke-like region. The image difference method is used to separate the moving pixels from the background. Moreover, setting particular gray-level range in RGB color model to define the smoke-like gray-level range and use the thresholding method to get the smoke-like region from the moving pixels. In the next step, use the optical flow method to analyze the motion of smoke and there are two more

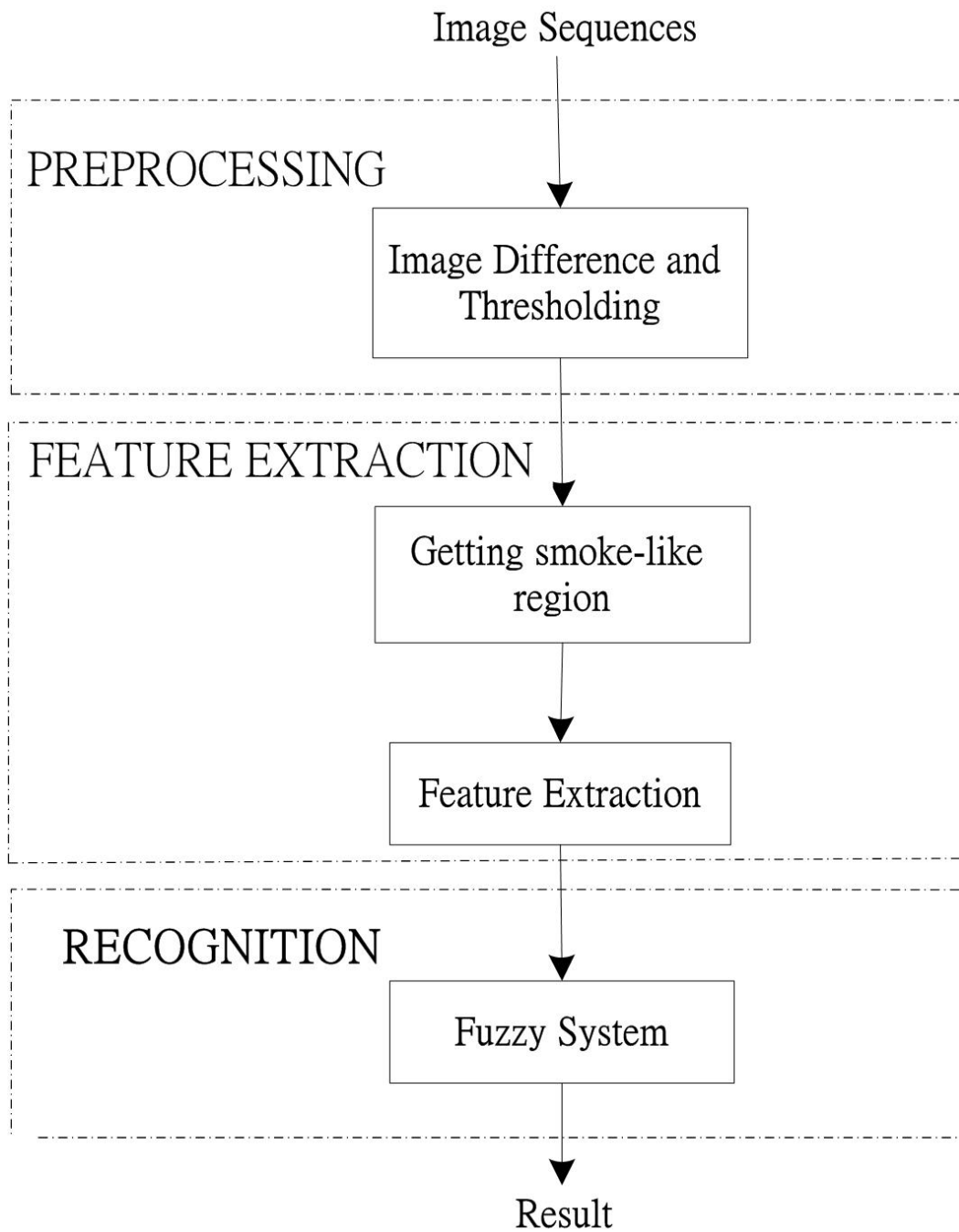


Fig. 3.1. The system architecture of the proposed approach.

properties accompanying with the smoke arising. First, when the combustible catch fires, smoke always produce at the same time and appear more and more in the scene. That's called *Spreading*. Second, smoke expands conjunctly. Although smoke will expand more and more, smoke region are almost still connected with each other. That's called *Connectivity*. Finally, the fuzzy inference system is used to utilize the three features to recognize the moving objects in the scene are smoke or not.

3.1 Preprocessing

In this section, the moving objects are separated from the background by using the image difference method. Moreover, to these moving objects, we set threshold to get the possible gray-level value of smoke in RGB color model. Then, the smoke-like pixels are separated from the background.



3.1.1 Defining the smoke-like color

In the RGB model, each color appears in its primary spectral components of red, green, and blue. This model is based on a Cartesian coordinate system. If the color of smoke is not influenced by the light of fire, it always appears from light gray to black. In RGB model, the gray scale (points of equal RGB values) extends from black to white along the diagonal line. Along the line, we dismiss from the too white and over black color and set a cylinder to fit in those conditions:

$$\begin{aligned}
 |R-G| &< \text{constant} \\
 |G-B| &< \text{constant} \\
 |B-R| &< \text{constant}
 \end{aligned} \tag{3.1}$$

If the pixel values fits in this range(Fig. 3.2), the pixel is considered as smoke-like pixel.

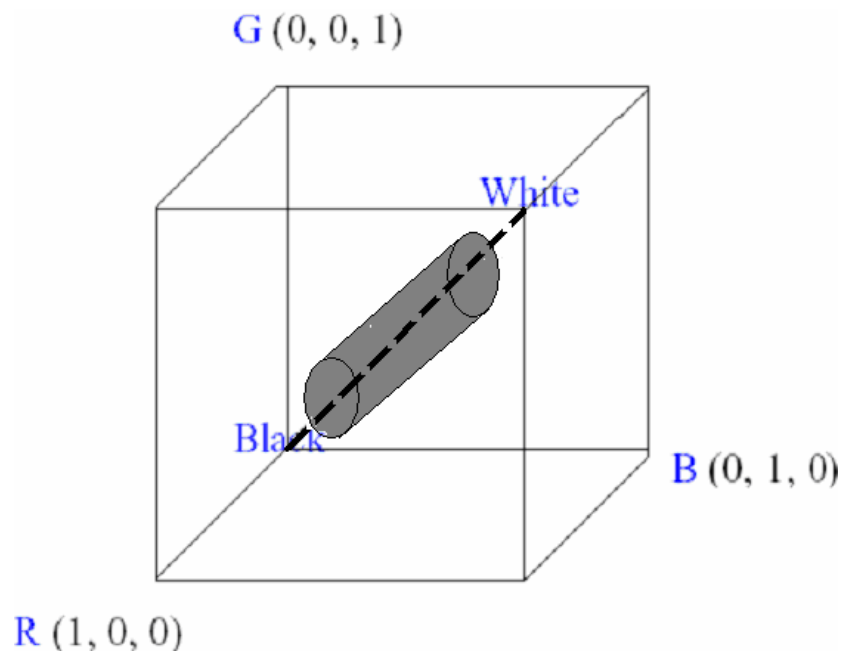


Fig. 3.2. The range of smoke color in RGB model

3.1.2 Image difference and thresholding

In order to obtain the moving smoke-like region in the scene. The first step we use the image difference to get the moving objects in the fixed scene. The second step, capture the smoke-like region from the moving object. Check every pixel that changing in the background. If the pixel does not belong to the range of smoke color set appointed, set the color of pixel black. The procedure is as follows:

```
for  $x = 1$  to width of image
  for  $y = 1$  to height to image
    if pixel  $p(x,y)$  does not belong the color set
      then set the pixel to black
```

Used for judging whether it is a range of smoke color set or not as follows : Checking on

pixel's RGB values whether it is in the designated threshold value range. If the pixel accord with the condition, the pixel color belong the smoke color set.

$$\text{if } (p(x,y,R) - p(x,y,G)) < \text{constant} \quad \text{and} \quad (p(x,y,G) - p(x,y,B)) < \text{constant}$$

$$\text{and } (p(x,y,B) - p(x,y,R)) < \text{constant} \quad \text{and} \quad 50 < p(x,y,I) < 240$$

then $p(x,y)$ belong to smoke color set

where $p(x,y,R)$ represents the red gray-value of the pixel (x,y) , $p(x,y,G)$ represents the green gray-value of the pixel (x,y) , $p(x,y,B)$ represents the blue gray-value of the pixel (x,y) , and $p(x,y,I)$ represents the brightness of the pixel (x,y) . The whole preprocessing is shown in Fig. 3.3 and Fig. 3.4.

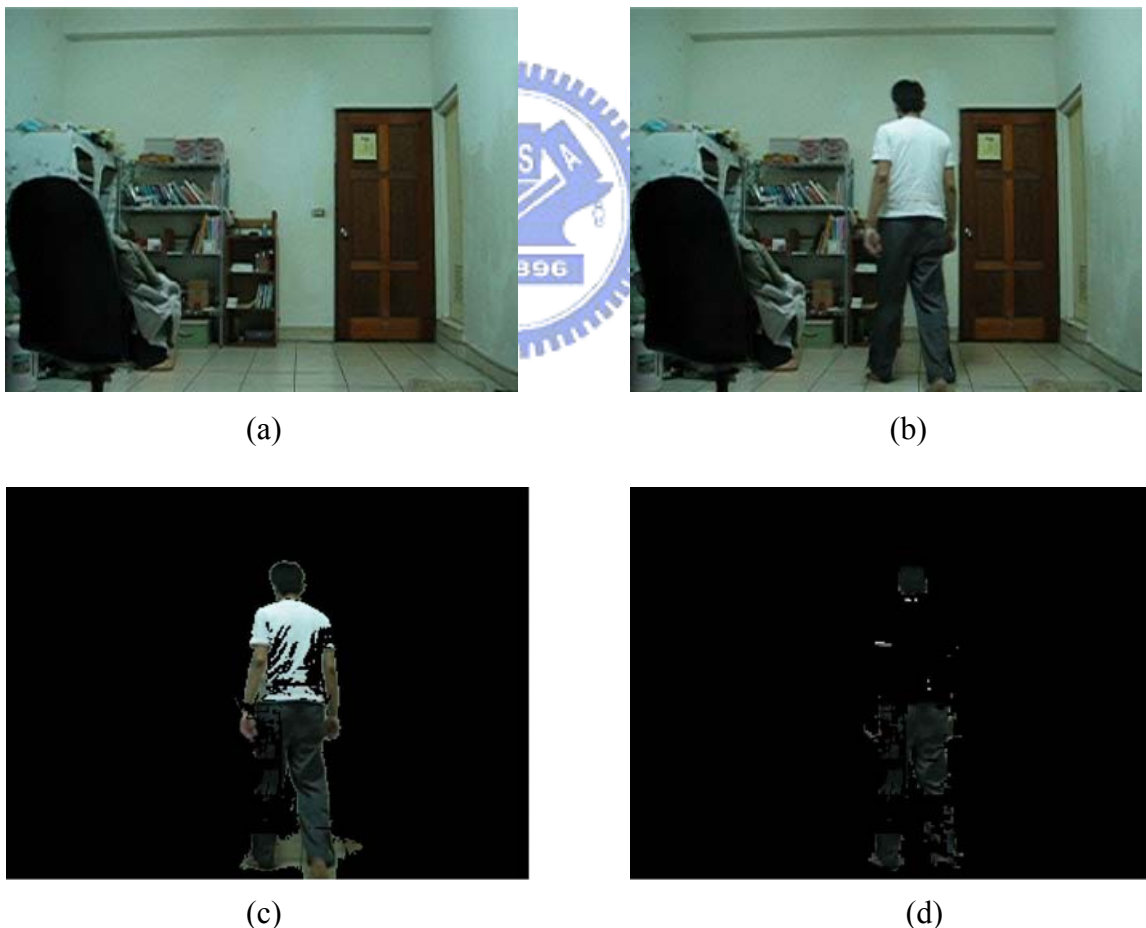


Fig. 3.3. Preprocessing(moving person). (a) background image (b) moving object in background (c) moving object (d) smoke-like region.

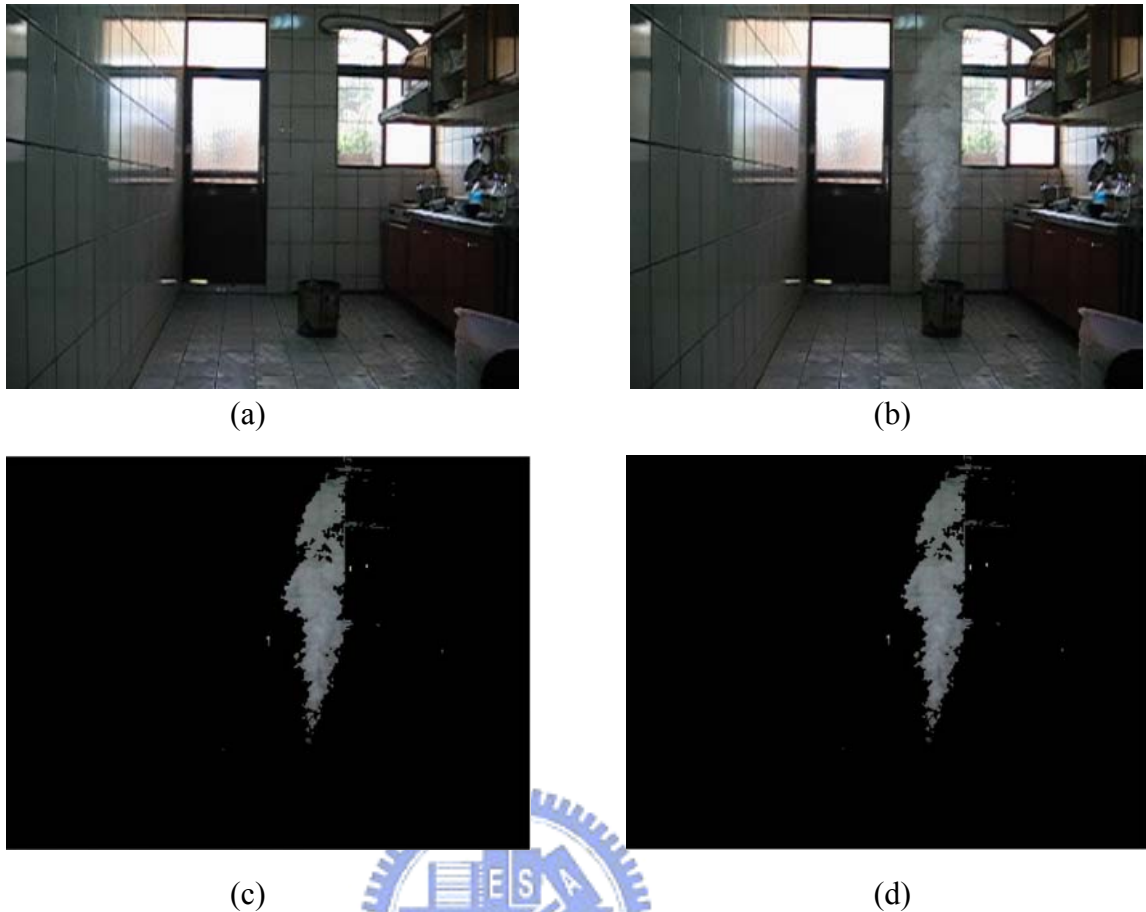


Fig. 3.4. Preprocessing (smoke). (a) background (b) moving object in background (c) moving object (d) smoke-like region

From Fig. 3.3 and Fig. 3.4, we can see the moving object is captured by using image difference method and the pixel color that doesn't belong to smoke-like color will be removed by color separation.

3.2 Feature Extraction

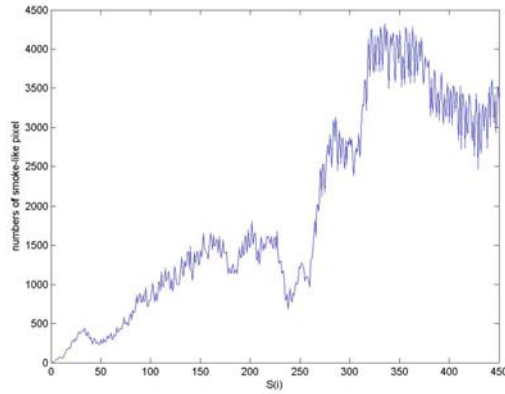
In this section, discuss about how to extract three characteristics of smoke. The gas, particle, aqueous vapor and ashes are following with what was produced by combustibles burning, fly away in the air, that is smoke which we saw. If the carbon of combustibles is richer, the smoke color will appear darker. On the other hand, if the carbon of combustibles is

poor, the smoke color will appear lighter. The vertical spreading speed of smoke is always larger than horizontal spreading speed because the aqueous in the smoke is lighter than air. So the smoke has characteristic of the upward movement continuously. Smoke is the same as the fire, both of them have the characteristic that will grow up and there is a characteristic of linking to each other in the growing up area. First of all, according to the growth situation of the smoke and characteristic that the smoke link to each other. We try to figure out the useful data that can be easily processed by artificial intelligence system and it will be introduced in section 3.2.1. Second, analyzing the sport situation within the smoke with the differential optical flow method. This is the most important characteristic of smoke and it will be introduced in section 3.2.2.

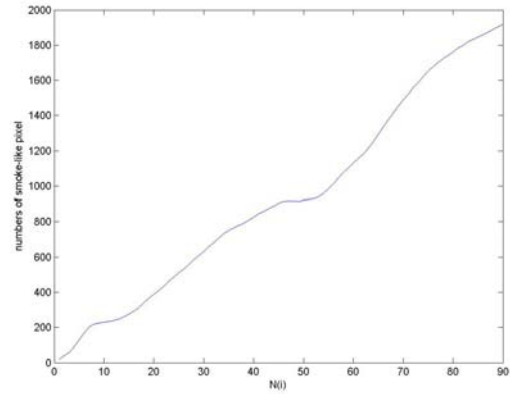
3.2.1 Spreading and Connectivity

Both of flame and smoke are the same, they have the characteristic of growing up and the characteristic of smoke is more obvious than the flame. One defect of visual fire detection is if the fire source is hided from the camera or IR camera, the flame won't be detected but the smoke has the strong spreading trend so that it is not easy to be covered. This is a obvious advantage on using the characteristic of smoke to prevent from fire accident. Moreover, there is connectivity while the smoke is spreading.

We can observe it and know how the spreading degree is from the situation what smoke-like pixel increases in a fixed period of time. First, we compute the quantity of smoke-like pixel in image which is one of the whole image sequences. Let S_i represent the quantity of smoke-like pixel in i th image. Although smoke will grow up, smoke-like pixels in the film will not appear the trend that there is increase at every moment. (see Fig 3.5 (a))



(a)



(b)

Fig. 3.5. (a)the quantity of smoke-like pixel in every picture. (b)spreading degree in fixed time.

We can find out the spreading degree through the equation (3.1).

$$N(j) = \frac{1}{5^*j} \sum_{i=1}^{j*5} S(i) \quad (3.1)$$

then use simple operation to process. The procedure is as follow:

```

for j = 1 to max(i)/5
  if N(j+1) > N(j)
    PSD = PSD+1;
  then PSD % = (PSD/end)*100 ;

```

where PSD means the percentage of spreading degree, if the PSD is lager, it shows the moving object accord with the characteristic spread even more.

About the connectivity, if the scene of the smoke producing in the open air, it can figure out the smoke has trend of growth and the smoke regions are linking to each other apparently. In order to tell the connectivity, we cut the image which is after preprocessing (like as Fig. 3.4 (d)) and make it consists of 4×4 block first. If there are eight more smoke-like pixels in this block, we set the value of the block is one, otherwise set the value of the block is zero. To illustrate this procedure let us consider Fig 3.6(a) where the white block shows the smoke-like region. As indicated in Section 2.1.1, the image difference method in a dynamic

imaging problem has the tendency to cancel all background regions, leaving only image elements that correspond to noise and to the moving object. The noise problem can be handled by equation (3.2)

$$\begin{aligned}
 &\text{if } B(x+1, y+1) = 0 \text{ and } B(x+1, y) = 0 \text{ and } B(x+1, y-1) = 0 \\
 &\quad \text{and } B(x-1, y+1) = 0 \text{ and } B(x-1, y) = 0 \text{ and } B(x-1, y-1) = 0 \\
 &\quad \text{and } B(x, y+1) = 0 \text{ and } B(x, y-1) = 0
 \end{aligned} \tag{3.2}$$

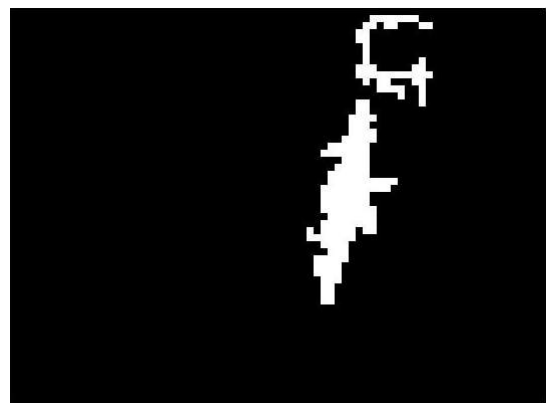
then

$$B(x, y) = 0$$

where $B(x,y)=1$ represents the block is a smoke-like region and $B(x,y)=0$ represents the block is not smoke-like region. After the process, see Fig 3.6(b). The independent block without linking to any block is canceled. Generally speaking, if there are less than four connective regions, the moving object is considered as has connectivity. The percentage of connectivity degree from image sequence can be obtained. For example, If there are total 500 images and just only 400 images of the moving objects has connectivity, the percentage of connectivity degree, PCD is 80%.



(a)



(b)

Fig. 3.6. (a)smoke-like region (b)smoke-like region without independent block.

3.2.2 Motion within the smoke

Because of the convection and vapor is lighter than air, the smoke always have the trend that rises upwards. This is the most important characteristic of smoke. Optical flow is a velocity field associated with brightness changes in the image and the brightness conservation assumption is often made in method for optical flow estimation, which states that brightness of an image of any point on the object is invariant under motion but in fact, the brightness of an image of any point on the moving object is not invariant. Therefore, the brightness of moving object internal will change and it cause that we can get the optical flow information of the moving object internal. Generally speaking, the motion vector in the moving object internal is not in the order even though the moving object has particular direction. In other words, if an object moves upward in the scene, a lot of motion vectors that direct upward on the edge of the moving object can be obtained but in the internal of moving object, the motion vector maybe won't direct upward orderly.

Horn and Schunck is one of the differential methods which hypothesize the irradiance $E(x,y,t)$ can be differentiated and satisfies the intensity constancy (2.4). Except for the intensity constancy equation, they introduced the global smoothness constraint. Usually the neighboring points of a moving object will have similar velocity as the moving object, or the velocities of points inside the object vary smoothly. The characteristics of smoke are very suitable for the two constrains. First, if the moving object is smoke, the velocity of smoke is not large so that it fits in the brightness conservation assumption. Second, in this case neighboring points on the object have similar velocities. Because of the two reasons, we choose the Horn and Schunk's method [11] to analyze the motion of the smoke.

PMUD is defined (percentage of motion upward degree) to tell the smoke characteristic from the smoke motion. First, we just need the optical flow value of moving object and count how many number of motion upward pixels. If the motion upward pixels are more than half moving pixel in one frame, this frame is considered as the trend of smoke motion. For example, if there are 80% frames have the trend of smoke motion, the PMUD is 80. Generally speaking, the motion situation within the moving object is not in the order even though the moving object has the particular motion direction. But the motion situation within the smoke has the trend that no matter what outside force influence the smoke motion, the internal smoke motion still has the trend of moving upward continuously. This is the most important characteristic of smoke and it is difference from the other moving object. In order to save computing time, we use 2×2 blocks or 4×4 blocks to represent a pixel and summarize every pixel's optical flow value to represent the block's motion vector. The optical flow field which is from two continuous frames mentioned on Fig 3.4 is shown in Fig 3.7. The procedure is as follows:

```

for  $i = 1$  to end
  if  $MU(i) > MD(i)$ 
     $MUD = MUD + 1$  ;

  then  $PMUD \% = (MUD/end)*100$  ;

```

Where $MU(i)$ represents the number of motion upward block in i th frame, $MD(i)$ represents the number of motion down block in i th frame and if the PMUD is larger, the possibility moving object is smoke is higher.

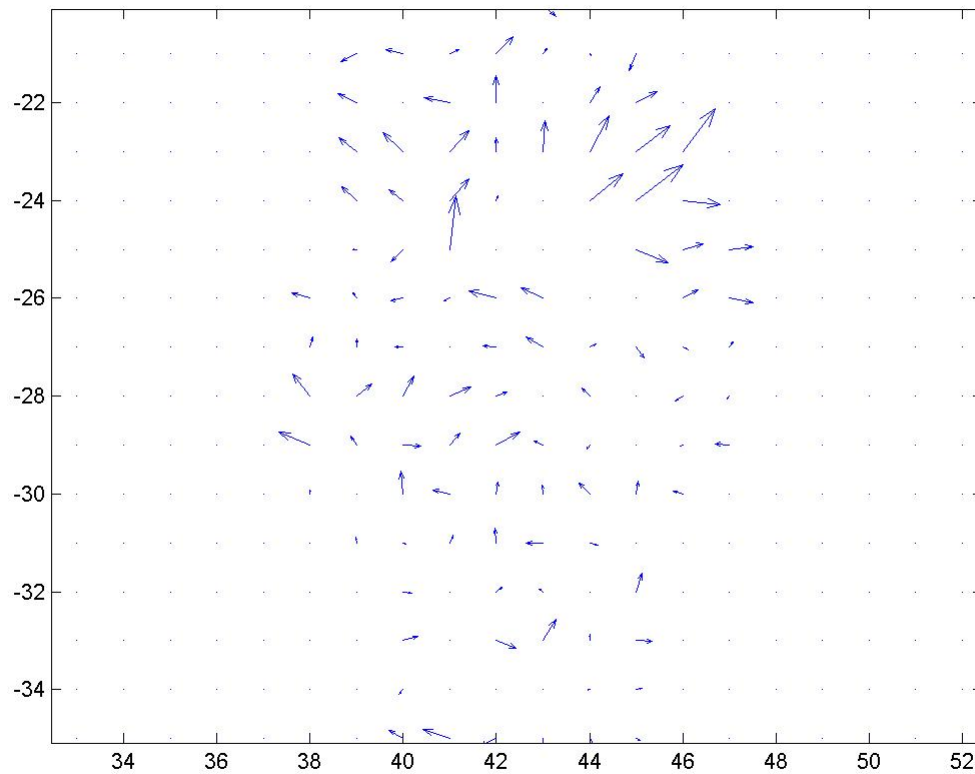


Fig. 3.7. Optical flow field from two continuous frames mentioned on Fig 3.4.



3.3 Fuzzy Inference System

Because of the fuzzy logic has the ability to express the amount of the ambiguity in human thinking and subjectivity in a comparatively undistorted manner, the fuzzy inference is applied to establish a fuzzy classifier which can classify the moving object is smoke or not. The concept of fuzzy inference is introduced in section 2.3. Here, three features which are described in the section 3.1 and 3.2 are assigned as the inputs of the fuzzy system. The three features are the percentage of spreading degree (PSD), the percentage of moving upward degree (PMUD), and the percentage of connectivity degree (PCD), respectively. The output is a value which indicates the possibility of smoke producing and is named after tendencious

possibility (TP). If the value of TP is closer to eight, the moving object tends to be smoke. On the other hand, if the value of TP is closer to minus eight, the moving object does not tend to be smoke. The input membership functions are seen in Fig. 3.8 to Fig. 3.10 and the output membership function is shown in Fig. 3.11. Moreover, the fuzzy rules are illustrated in Table 3.1.

The membership function of the high separating rate has a stricter toleration of the distortion than the membership function of the low separating rate. Therefore, the membership function of the high separating rate are used and the high separating rate means that the overlapping area of neighboring parts in the membership function is smaller than that in the low separating rate. For the input membership function of PMUD which is shown in Fig. 3.8. The region of PMUD is divided into three parts and if the value in the axle of SDCG is lager, the tendence of the smoke will be more obvious. For the input membership function of PSD which is shown in Fig. 3.9. The region of PSD is divided into three parts and if the value in the axle of PSD is lager, the tendence of the smoke will be more obvious. For the input membership function of PCD which is shown in Fig. 3.10. The region of PCD is divided into two parts and if the value in the axle of PCD is larger, the tendence of smoke will be more obvious. For the output membership function of TP which is shown in Fig. 3.11. The region of TP is divided into five parts and if the value in axle of PMUD, the most important characteristic of smoke is lager, the tendence of smoke will be more obvious. According to the combination of input membership functions, the fuzzy rules are illustrated in Table 3.1 and discrimination results can be gotten based on these rules.

In the following, an example is shown to explain how to detect smoke producing. Let's see Fig. 4.5, Fig. 4.7 and put the emphasis on three characteristics. The value of PMUD of

the two image sequences are 76.33 and 52.46, respectively. The values of PSD of the two image sequences are 98 and 63.23, respectively. Moreover, the values of PCD of the two image sequences are 88 and 50.58, respectively. Then according to the fuzzy rules, the tendencious

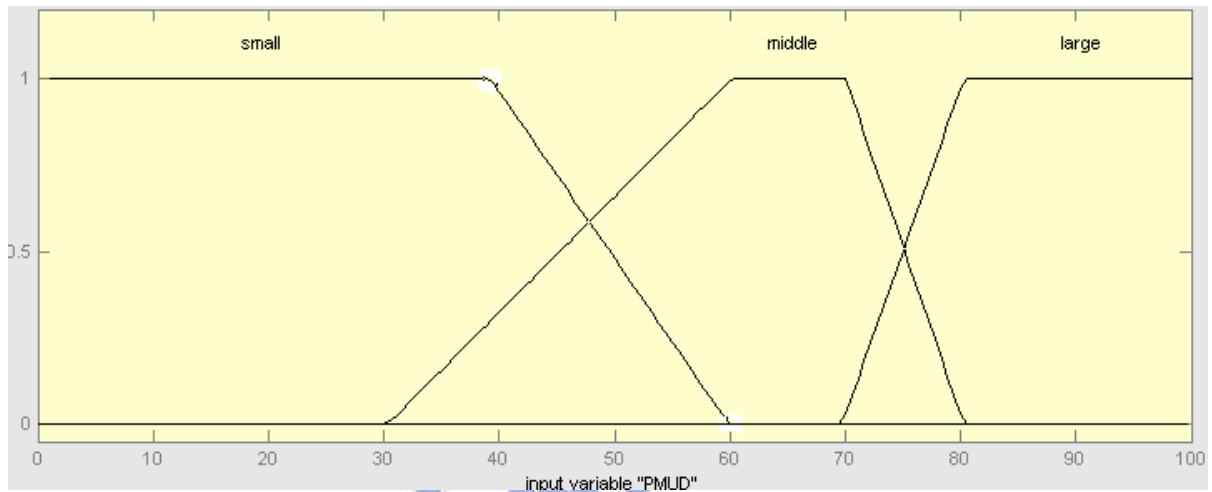


Fig. 3.8. Membership function of the percentage of motion upward degree.

possibility is computed. First, the firing strength of Rule 1 for *VeryDangerous* is calculated by

$$\alpha_1 = \min (\text{large}(\text{PMUD}), \text{large}(\text{PSD}), \text{high}(\text{PCD})) = 0.633$$

where

$$\text{large}(\text{PMUD}) = \frac{(76.33 - 70)}{(80 - 70)} = 0.633 \text{ , and}$$

$$\text{large}(\text{PSD}) = 1 \text{ , and}$$

$$\text{large}(\text{PCD}) = 1.$$

And similarity for Rule 7, the firing strength is

$$\alpha_2 = \min (\text{middle}(\text{PMUD}), \text{large}(\text{PSD}), \text{high}(\text{PCD})) = 0.367$$

where

$$\text{middle(PSD)} = \frac{(80 - 76.33)}{(80 - 70)} = 0.367, \text{ and}$$

$$\text{large(PSD)} = 1, \text{ and}$$

$$\text{large(PCD)} = 1.$$

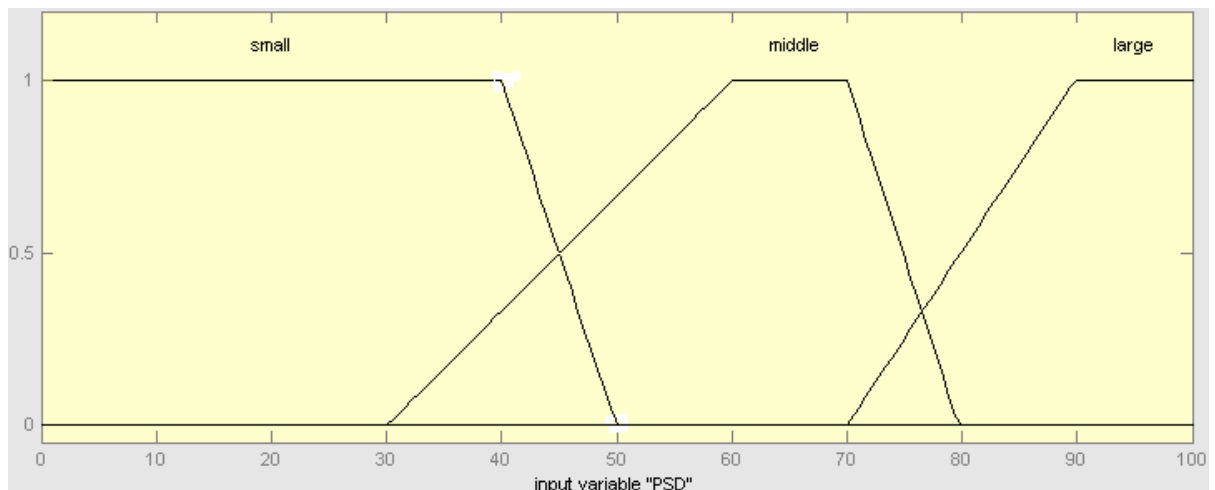


Fig. 3.9. Membership function of the percentage of spreading degree.

Moreover, the firing strengths for the other 8 rules are 0. Then the defuzzified value for the conclusion is obtained

$$z_{COA} = \frac{(6) \times (0.633) + (4) \times (0.367)}{0.633 + 0.367} = 5.266$$

If the defuzzified value is smaller than 2, the moving object won't be considered as smoke. If the defuzzified value is not smaller than 2, the moving object will be considered as smoke. The possibility that moving object is smoke is higher, the defuzzified value is closer to 8. Similarly, the defuzzified value for the moving object in Fig. 4.3 image sequences can be calculated and the value is -0.9375. Therefore the moving object is not smoke.

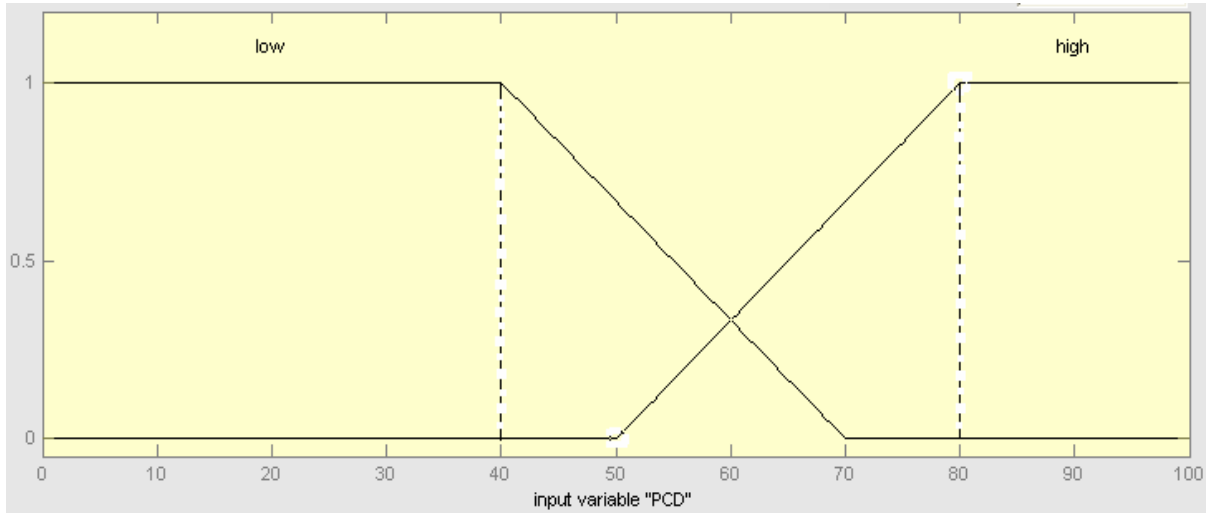


Fig. 3.10. The membership function of the percentage of connectivity degree.

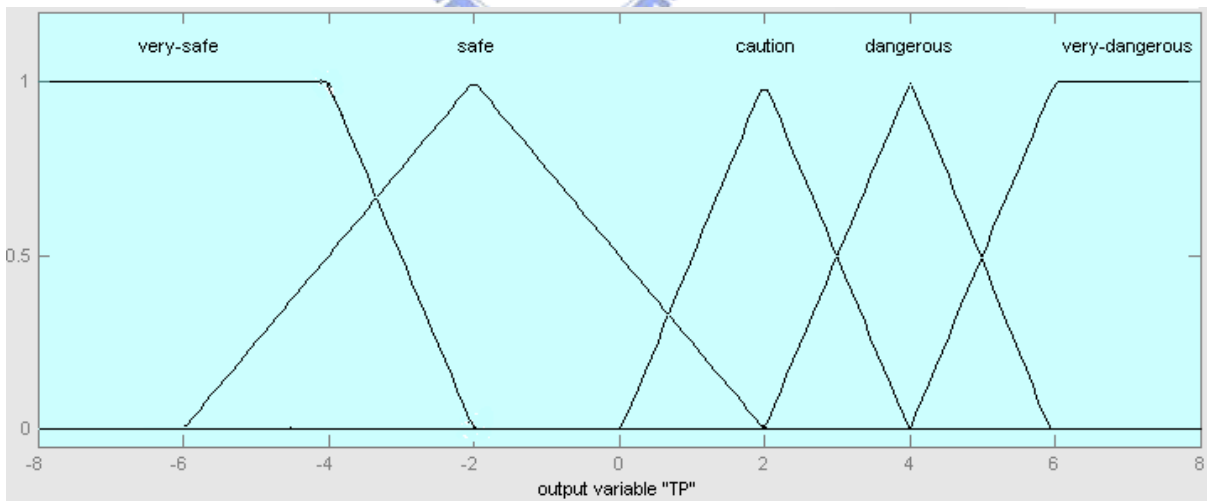


Fig. 3.11. Membership function of the tendencious possibility of smoke producing.

Table. 3.1. Fuzzy rule.

Rule	If <i>PMUD</i> is	and	<i>PSD</i> is	and	<i>PCD</i> is	Then <i>TP</i> is
1	<i>large</i>		<i>large</i>		<i>high</i>	<i>very dangerous</i>
2	<i>large</i>		<i>large</i>		<i>low</i>	<i>dangerous</i>
3	<i>large</i>		<i>middle</i>		<i>high</i>	<i>dangerous</i>
4	<i>large</i>		<i>middle</i>		<i>low</i>	<i>dangerous</i>
5	<i>large</i>		<i>small</i>		<i>high</i>	<i>caution</i>
6	<i>large</i>		<i>small</i>		<i>low</i>	<i>caution</i>
7	<i>middle</i>		<i>large</i>		<i>high</i>	<i>dangerous</i>
8	<i>middle</i>		<i>large</i>		<i>low</i>	<i>caution</i>
9	<i>middle</i>		<i>middle</i>		<i>none</i>	<i>safe</i>
10	<i>small</i>		<i>none</i>		<i>none</i>	<i>very safe</i>

PMUD : Percentage of motion upward degree.

PSD : Percentage of spreading degree.

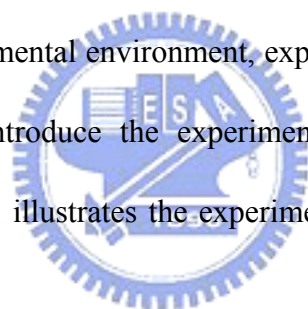
PCD : Percentage of connectivity degree.

TP : Tendencious possibility.

Chapter 4

Experiments and Discussions

In this chapter, the experimental environment, experiment results, and the application are described. In section 4.1, introduce the experiment environments, includes indoor and outdoor scene. In section 4.2, illustrates the experimental results. Finally, Section 4.3 deals with discussions.



4.1 Experimental Environments

For experimenting image-based smoke detection, the video sequences shot by the DV8 camera. The video sequences are made in the form of 320 pixels \times 240 pixels. The experiment scene is divided into indoor and outdoor. The indoor image sequences are smoke producing in the kitchen, staircase and cigarette smoke. The outdoor image sequences are the chimney discharges the smoke and smoke producing by the roadside. The places are chosen for different kinds of moving object and different background. Smoke, people and

motorcycles are playing the roles of moving objects. The optical flow fields are represented as a needle diagram. The estimated flow velocities are depicted as short line, showing the apparent displacement during one time step.

4.2 The Experimental Results

The experiment is divided into two parts. The algorithm as described in Chap 3 was tested on indoor image sequences discussed in Section 4.2.1. The algorithm as described in Chap 3 was tested on outdoor image sequences discussed in Section 4.2.2.

4.2.1 Indoor image Sequences

In this section, using the indoor image sequences tests the algorithm in Chap 3. The experiment moving objects are divided into smoke and people. Among the people's motion, are split into moving horizontally and moving vertically. The first experiment is producing smoke in the kitchen. The defuzzified value is 6.45. It is closed to 8 so that we think the moving object in the scene is smoke. The original image sequences are shown in Fig. 4.1. Figure Fig. 4.2 shows the most important characteristic of smoke, the motion upward within smoke and optical flow fields obtained from the image sequence shown in Fig. 4.1 by the Horn and Schunck algorithm. The Horn and Schunck method used $\alpha=1.5$, and the number of iteration is 5. We do not have to spend too much time on iteration to obtain the precise optical flow value because obtaining the motion direction is more important to us. The blue part of pie chart in Fig. 4.2 shows the percentage of motion upward pixel.

The second experiment is a person goes up stair in the kitchen. This experiment is trying to simulate gray object move upward just like as smoke. The defuzzified value is -1.43. It is far away 8 so that we think the moving object in the scene is not smoke. The original image sequences are shown in Fig. 4.3. Figure Fig. 4.4 shows the optical flow fields of moving object internal and the pie chart shows the percentage of motion upward pixel.

The third experiment is three people go up in the staircase. This experiment is trying to simulate object move upward and more and more smoke-like color object show up in the scene. The defuzzified value is -0.36. It is far away from 8 so that we think the moving object is not smoke. The original image sequences are shown in Fig. 4.5. Figure Fig. 4.6 shows the optical flow fields of moving object internal and the pie chart shows the percentage of motion upward pixel.

The fourth experiment is smoke produced in the kitchen and shoot from further place. This experiment is similar as first experiment but shoot from further place. The smoke size in the scene is smaller than first one and defuzzified value is 5.69. It is still closed to 8 so that we think the moving object is smoke. The original image sequences are shown in Fig. 4.7. Figure Fig. 4.8 shows the enlarged optical flow fields of moving object internal and the pie chart still shows the percentage of motion upward pixel.

The fifth experiment is smoke produced at staircase. The smoke color is similar as background color in this experiment so that clear smoke motion can't be captured by preprocessing. The estimation of PMUD is influenced seriously. The defuzzified value is -2.133. It is not closed to 8 so that the moving object is not considered as smoke. The original image sequences are shown in Fig. 4.9. Figure Fig. 4.10 shows the enlarged optical flow fields of moving object internal and the pie chart still shows the percentage of motion upward

pixel.

The sixth experiment is smoke produced while burning from cigarette shoot at short range. This experiment is for observing the smoke motion and emphasized on PMDU condition so that we do not consider PSD and PCD. The PMDU of this experiment is 78.46%. The original image sequences are shown in Fig. 4.11. Figure Fig. 4.12 shows the enlarged optical flow fields of moving object internal and the pie chart still shows the percentage of motion upward pixel.

Totally speaking, in indoor environment, although the quantity of smoke is not a lot, smoke is not influenced on wind force. The visibility of smoke is still good enough to recognize but when smoke color is similar as background color, it is difficult to capture clear motion of smoke so that system can't detect smoke successfully. People are the most moving objects in indoor environment and the system can discriminate between smoke and people by PMUD.

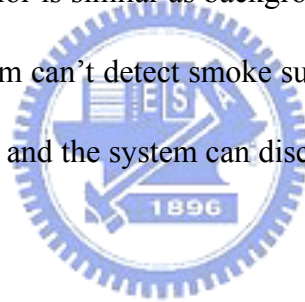


Table. 4.1. Three kinds of degree and defuzzified value in indoor scene.

	PMUD	PSD	PCD	Defuzzified Value
First experiment	91.43 %	98.88 %	99.77 %	6.45
Second experiment	59.24 %	71.11 %	26.48 %	-1.43
Third experiment	50.22 %	80.00 %	75.88 %	-0.36
Fourth experiment	77.56 %	76.00 %	75.11 %	5.69
Fifth experiment	52.67 %	80.00 %	40.22 %	-2.13



(a)



(b)



(c)



(d)



(e)



(f)



(g)



(h)

Fig. 4.1. Smoke produced in a kitchen. (a) Frame 50. (b) Frame 100. (c) Frame 150. (d) Frame 200. (e) Frame 250. (f) Frame 300. (g) Frame 350. (h) Frame 450.

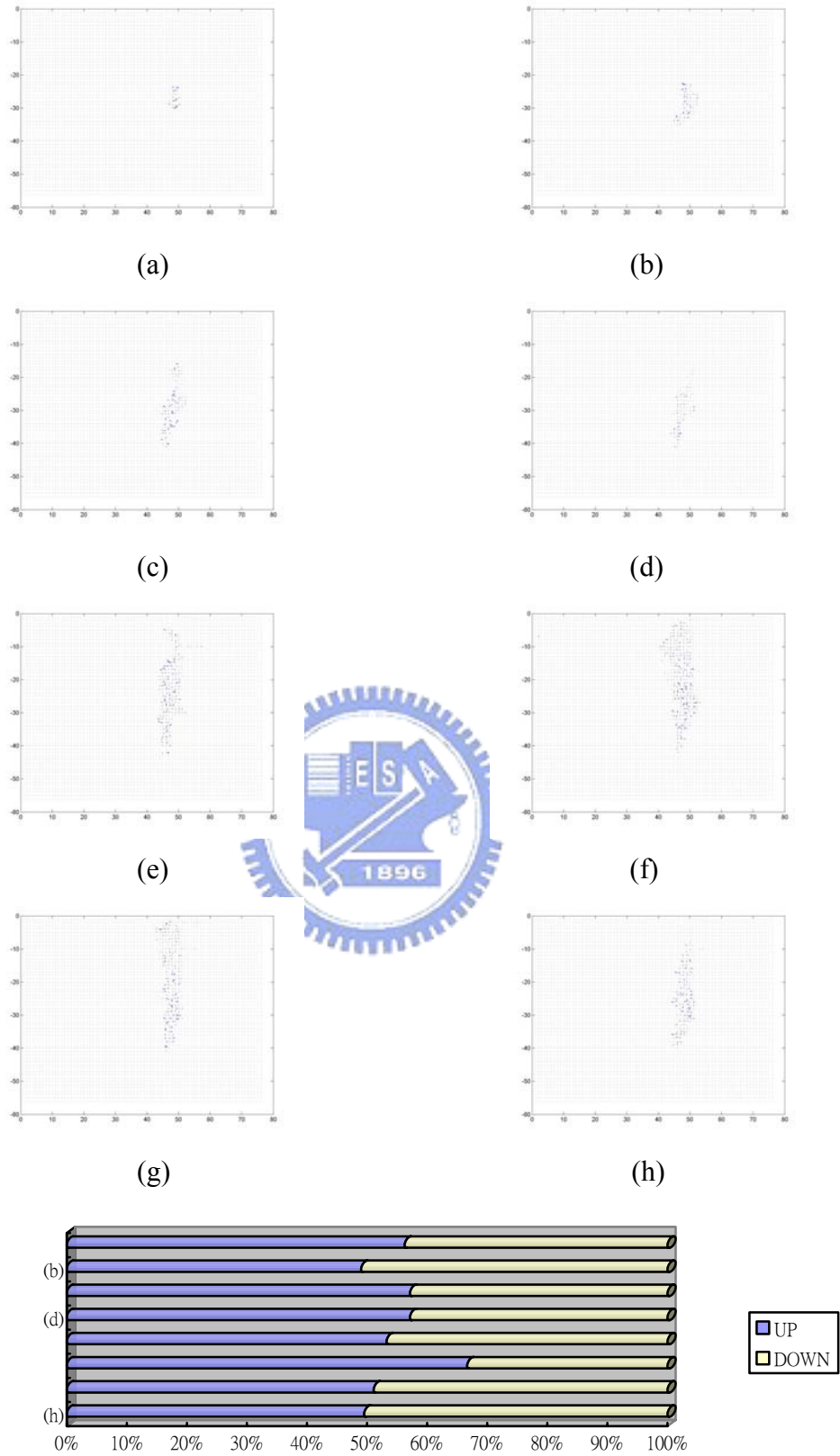


Fig. 4.2. Flow fields applied to smoke producing in a kitchen sequences and the blue part of bar chart shows the percentage of motion upward pixel. Frame number is the same as Fig. 4.1.

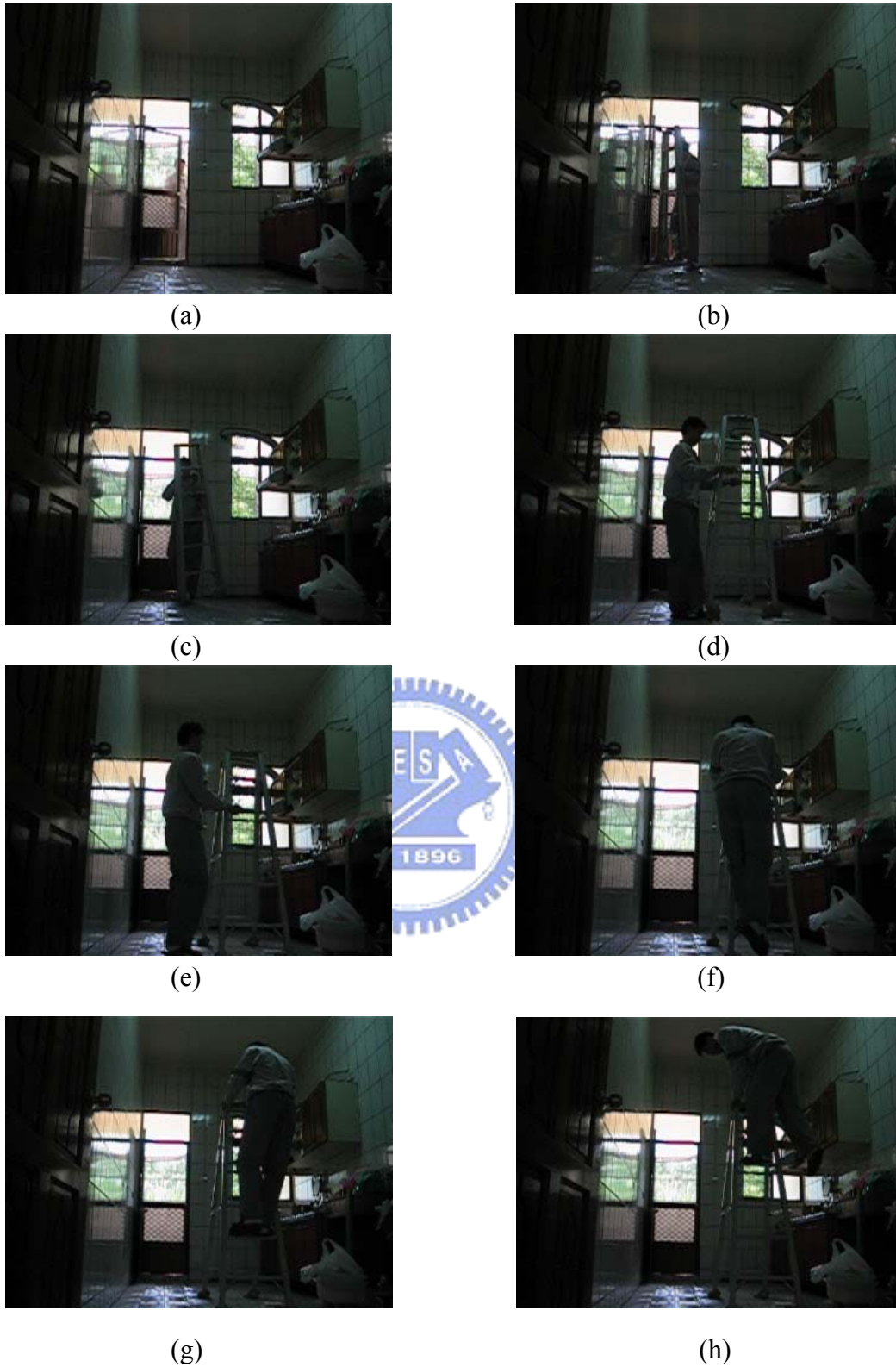


Fig. 4.3. A gray person goes up stair in the kitchen. (a) Frame 50. (b) Frame 100. (c) Frame 150. (d) Frame 200. (e) Frame 250. (f) Frame 300. (g) Frame 350. (h) Frame 450.

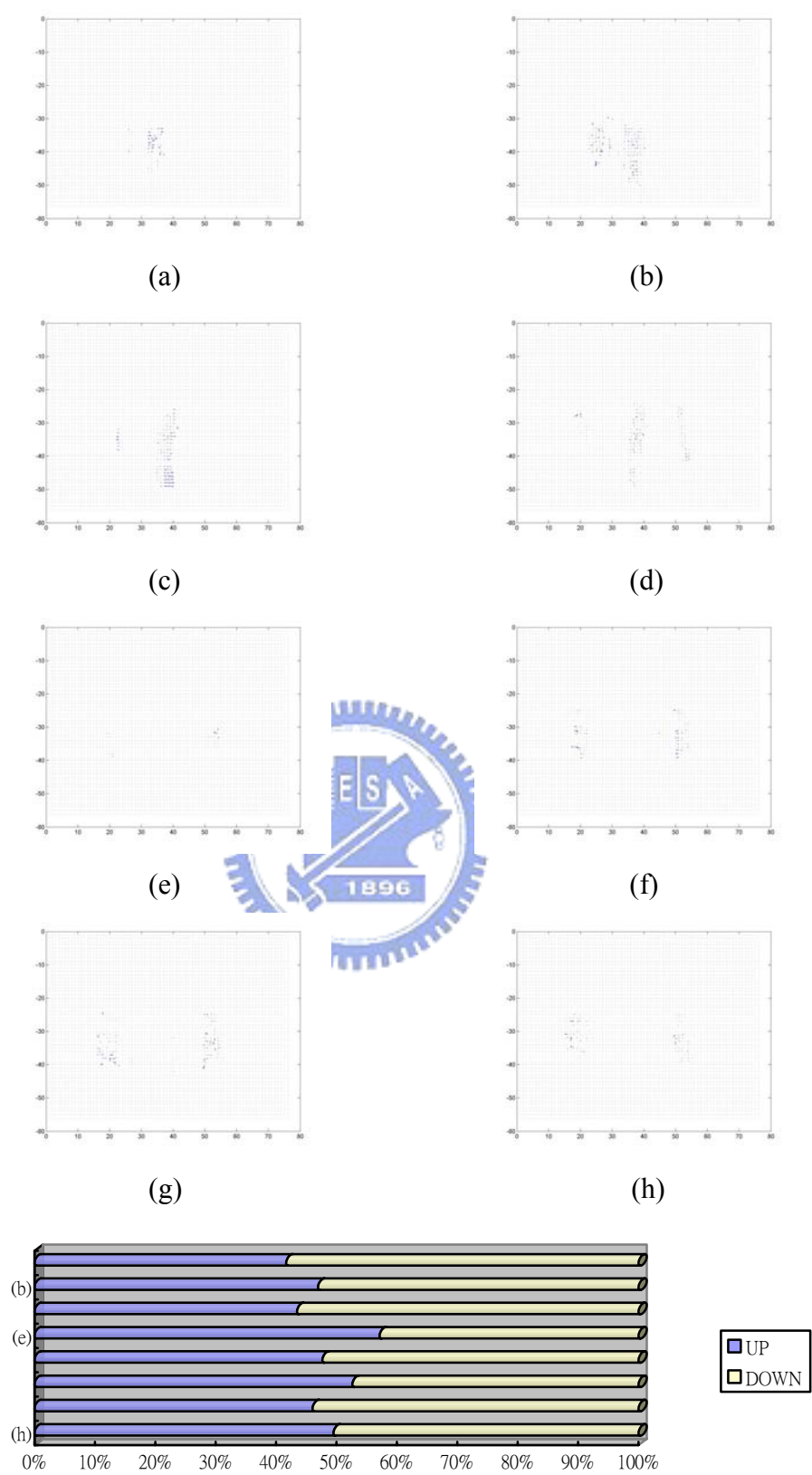


Fig. 4.4. Flow fields applied to gray person goes up the stair in the kitchen sequences and the blue part of bar chart shows the percentage of motion upward pixel. Frame number is the same as Fig. 4.3.



Fig. 4.5. Three people go up in the staircase. (a) Frame 50 (b) Frame 100 (c) Frame 150 (d) Frame 200 (e) Frame 250 (f) Frame 300 (g) Frame 350 (h) Frame 450.

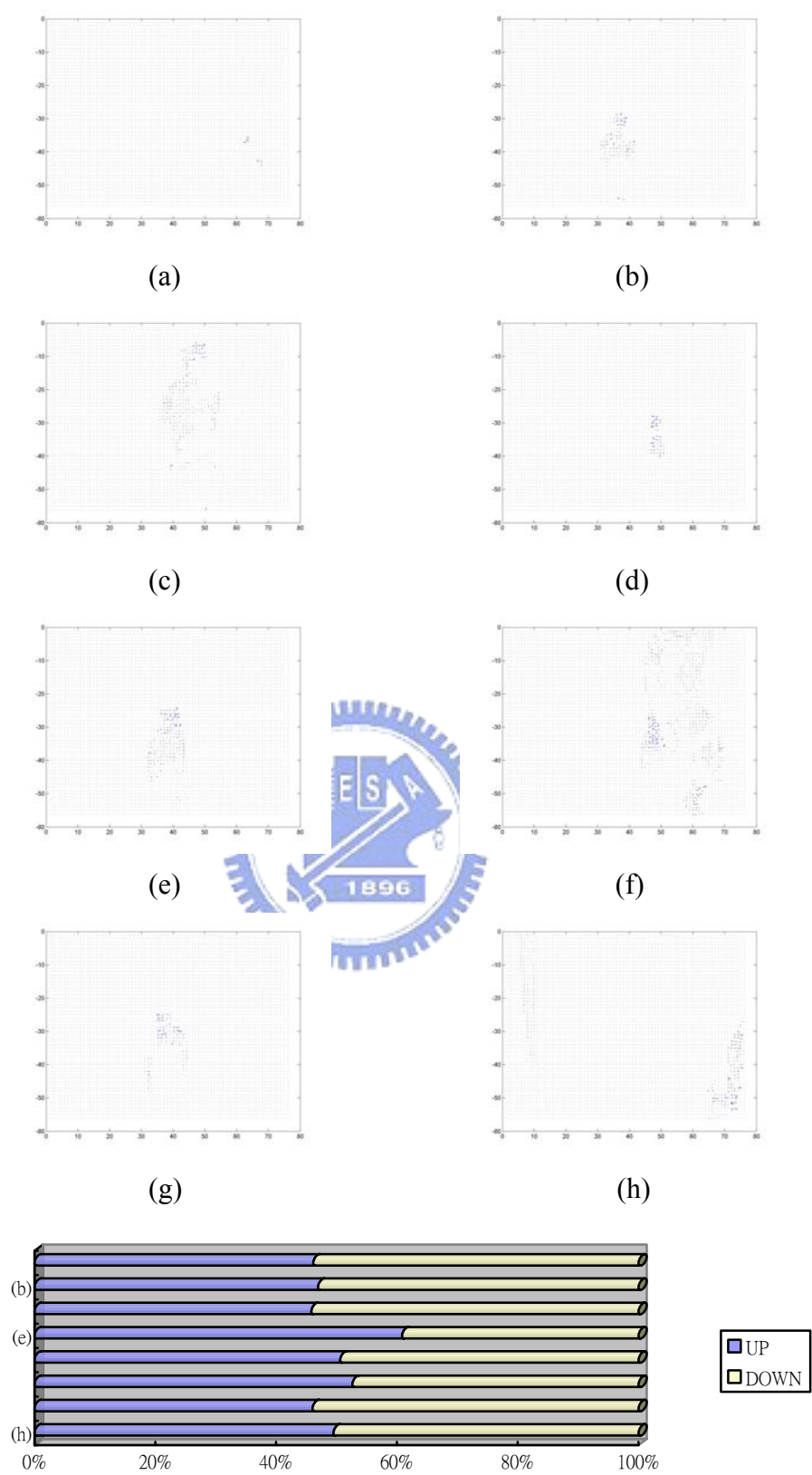


Fig. 4.6. Flow fields applied to three person goes up in the staircase sequences and the blue part of bar chart shows the percentage of motion upward pixel. Frame number is the same as Fig. 4.5.



(a)



(b)



(c)



(d)



(e)



(f)



(g)



(h)

Fig. 4.7. Smoke produced in a kitchen shoot from distant place. (a) Frame 50. (b) Frame 100. (c) Frame 150. (d) Frame 200. (e) Frame 250. (f) Frame 300. (g) Frame 350. (h) Frame 450.

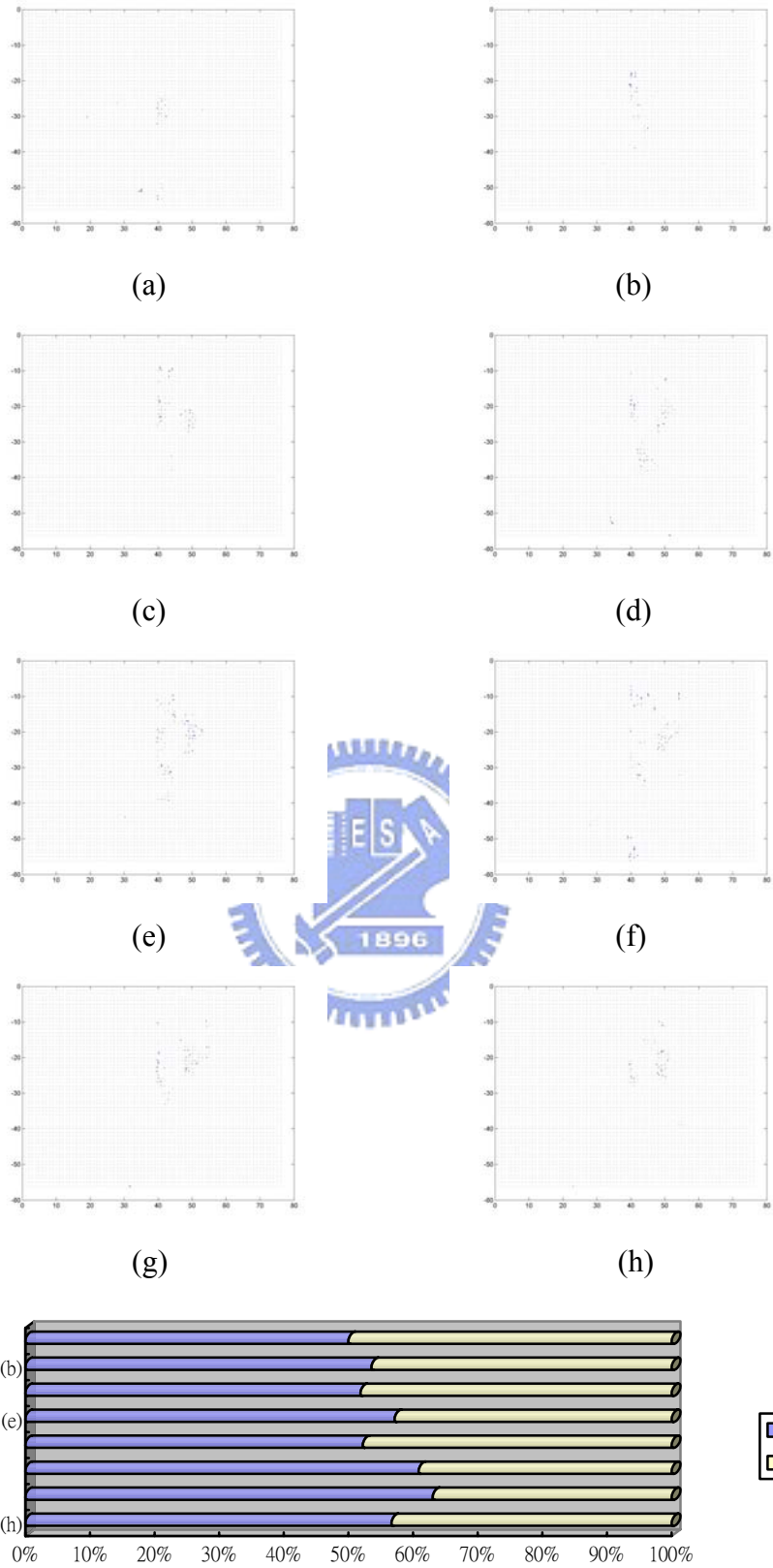


Fig. 4.8. Flow fields applied to smoke producing in a kitchen shoot from distant place sequences and the blue part of pie chart shows the percentage of motion upward pixel. Frame number is the same as Fig. 4.7.



(a)



(b)



(c)



(d)



(e)



(f)



(g)



(h)

Fig. 4.9. Smoke produced at staircase. (a) Frame 50. (b) Frame 100. (c) Frame 150. (d) Frame 200. (e) Frame 250. (f) Frame 300. (g) Frame 350. (h) Frame 450.

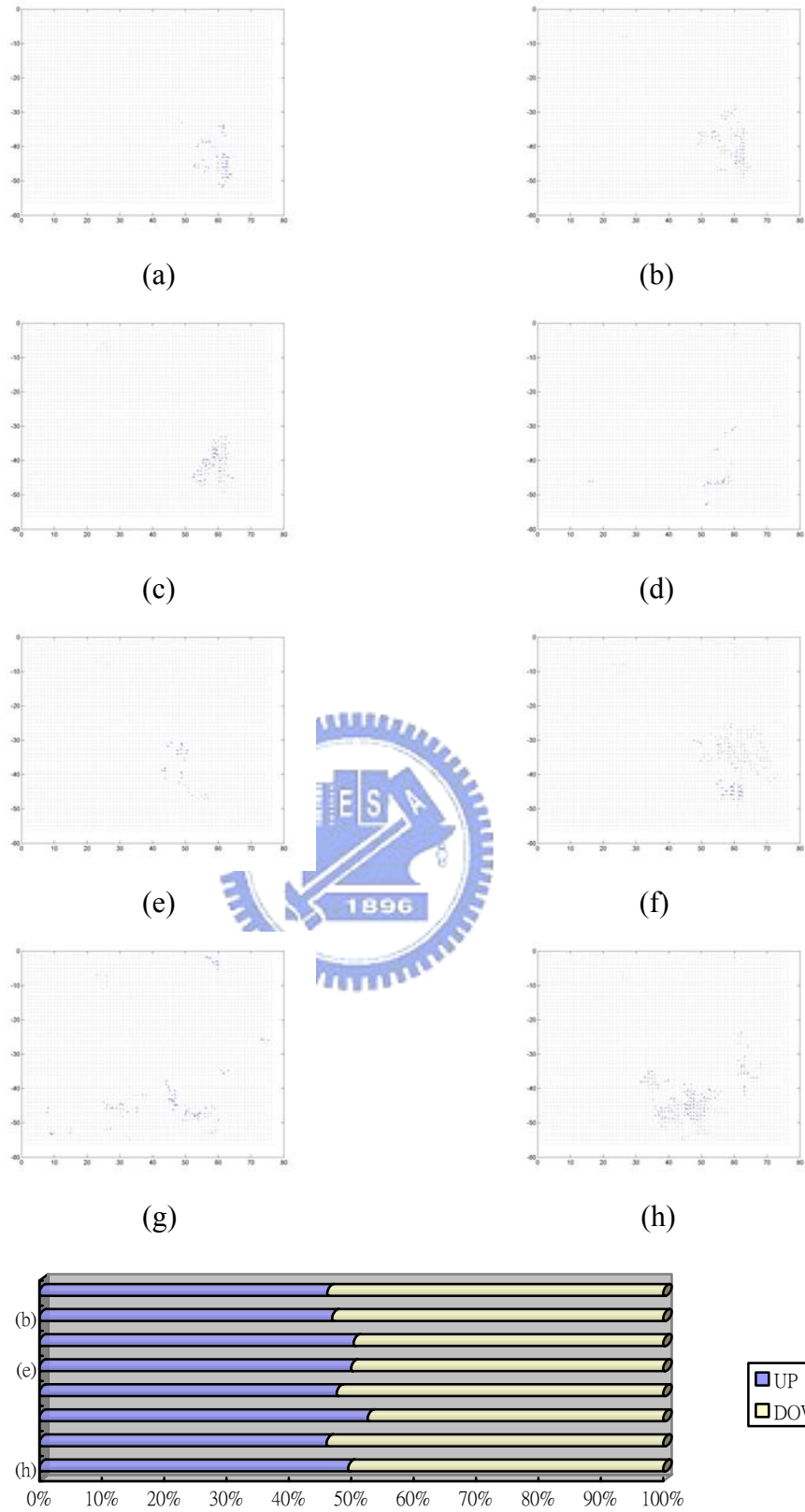


Fig. 4.10. The optical flow fields of moving object internal and the bar chart still shows the percentage of motion upward pixel. Frame number is the same as Fig. 4.9.

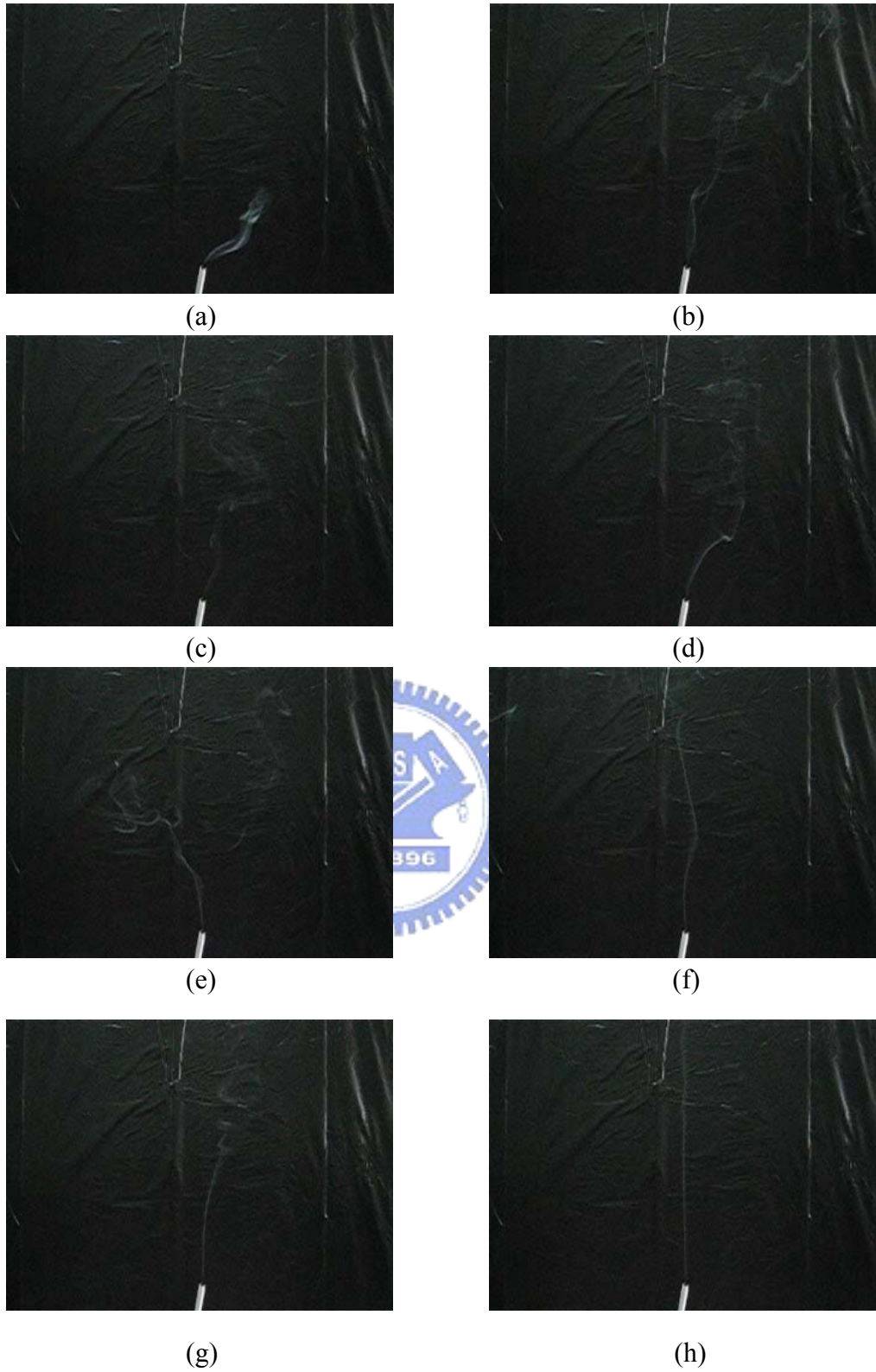


Fig. 4.11. Smoke produced while burning from cigarette shoot at short distant. (a) Frame 50. (b) Frame 100. (c) Frame 150. (d) Frame 200. (e) Frame 250. (f) Frame 300. (g) Frame 350. (h) Frame 450.

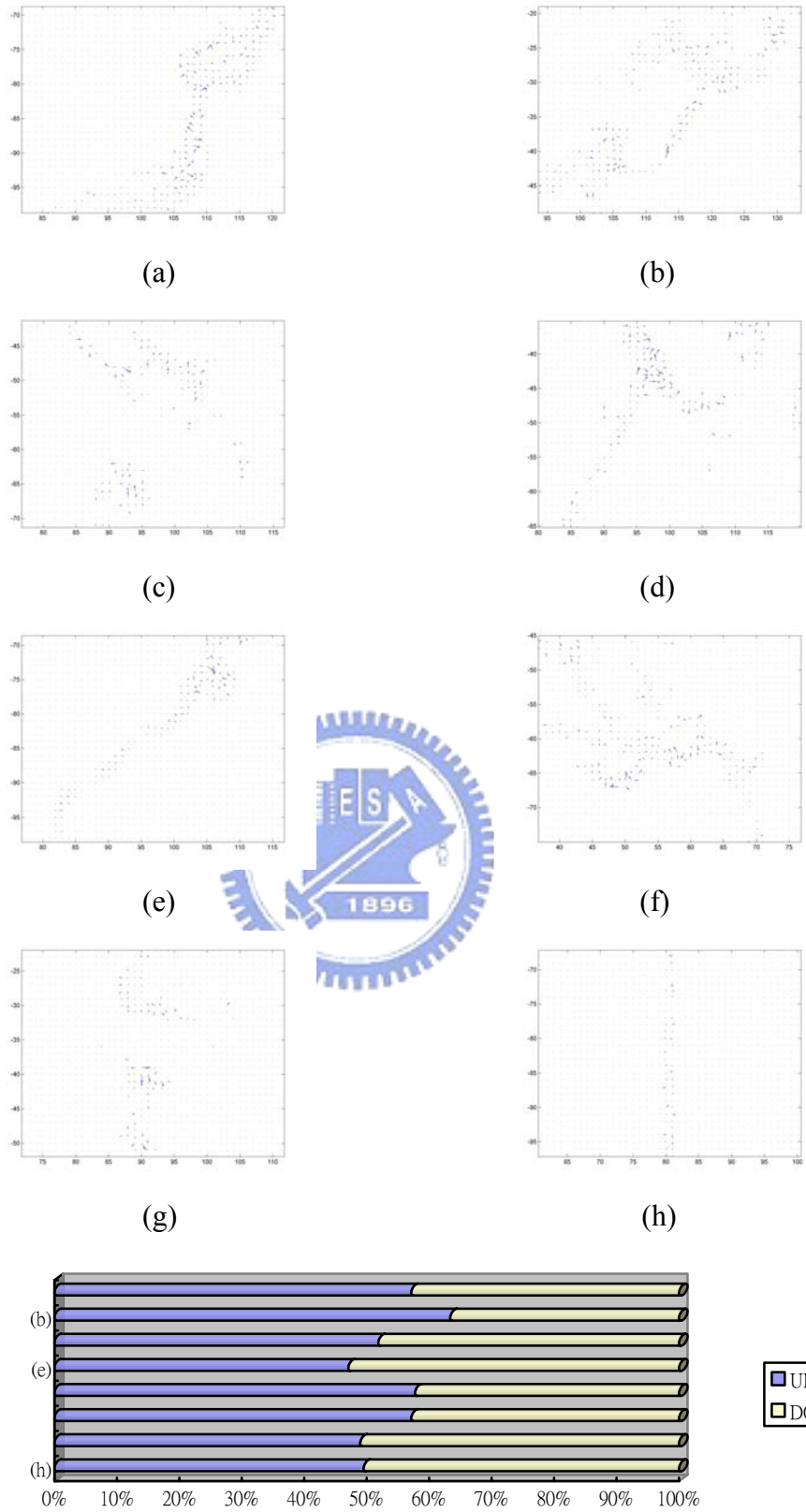


Fig. 4.12. Flow fields applied to Smoke produced while burning from cigarette shoot at short distant sequences and the blue part of pie chart shows the percentage of motion upward pixel. Frame number is the same as Fig. 4.11.

4.2.1 Outdoor image Sequences

In this section, using the outdoor image sequences tests the algorithm in Chap 3. There are some differences between indoor scene and outdoor scene. Because of considering the safety reason, we won't produce a lot of smoke indoor and if the quantity of smoke is not enough, the visibility of the smoke is influenced by wind-force easily. We can see the smoke is influenced by wind-force on outdoor scene. The first experiment is smoke produced on the roadside. Smoke is easy to be influenced by wind-force in this environment. The defuzzified value is 6.41. It is closed to 8. We think the moving object is smoke. The original image sequences are shown in Fig. 4.13. Figure Fig. 4.14 shows the optical flow fields of moving object internal and the pie chart shows the percentage of motion upward pixel.

The second experiment is people walk on the roadside and the scene is the same as the first experiment. The defuzzified value is -0.8932. It is not closed to 8. We think the moving object is smoke. The original image sequences are shown in Fig. 4.15. Figure Fig. 4.16 shows the optical flow fields of moving object internal and the pie chart shows the percentage of motion upward pixel.

The third experiment is people burn dried straw on the countryside. We miss initial stage of smoke producing but the PSD is still obvious. The defuzzified value is 6.45. It is closed to 8. We think the moving object is smoke. The original image sequences are shown in Fig. 4.17. Figure Fig. 4.18 shows the optical flow fields of moving object internal and the pie chart shows the percentage of motion upward pixel.

The fourth experiment is the smoke which is discharged by chimney. This experiment is for observing the smoke motion and emphasize on PMDU condition so that we do not consider PSD and PCD. The PMDU of this experiment is 88.43%. The original image

sequences are shown in Fig. 4.19. Figure Fig. 4.20 shows the enlarged optical flow fields of moving object internal and the pie chart still shows the percentage of motion upward pixel.

The fifth experiment is the smoke which is discharged by chimney in strong wind situation. In this experiment, we also emphasize on PMDU and observe the difference between smoke in the strong wind situation and not in the wind situation. The PMUD is 77.23%. We can know wind will make influence upon smoke motion upward. The original image sequences are shown in Fig. 4.23. Figure Fig. 4.24 shows the enlarged optical flow fields of moving object internal and the pie chart still shows the percentage of motion upward pixel.

The sixth experiment is the smoke which is discharged by chimney in strong wind situation and motion of cloud is similar as smoke. The original image sequences are shown in Fig. 4.21. Figure Fig. 4.22 shows the enlarged optical flow fields of moving object internal and the pie chart still shows the percentage of motion upward pixel.

Totally speaking, in outdoor environment, many objects are moving in the scene and some moving objects color are similar as smoke, like cloud. The moving speed of cloud is very slow generally but sometimes the cloud will influence the detection result. There will be an important issue that how to discriminate between cloud and smoke. About other moving objects, it is possible to discriminate from the color characteristic of smoke.

Table. 4.2. Three kinds of degree and defuzzified value in outdoor scene.

	PMUD	PSD	PCD	Defuzzified Value
First experiment	92.22 %	98.89 %	74.22 %	6.41
Second experiment	55.56 %	97.77 %	1.33%	-0.89
Third experiment	99.56 %	98.89 %	98.89 %	6.48

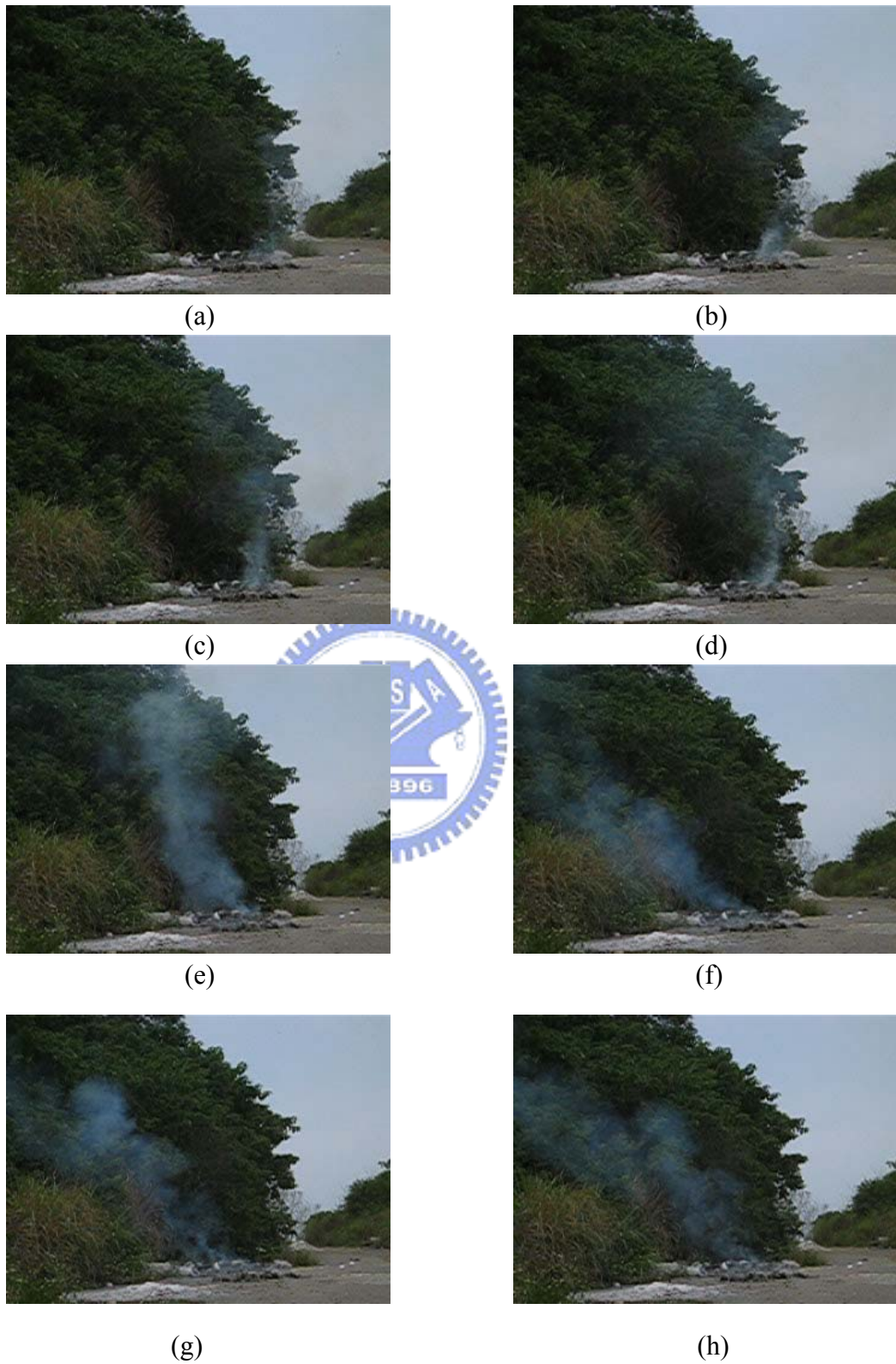


Fig. 4.13. Smoke produced on the roadside. (a) Frame 50. (b) Frame 100. (c) Frame 150. (d) Frame 200. (e) Frame 250. (f) Frame 300. (g) Frame 350. (h) Frame 450.

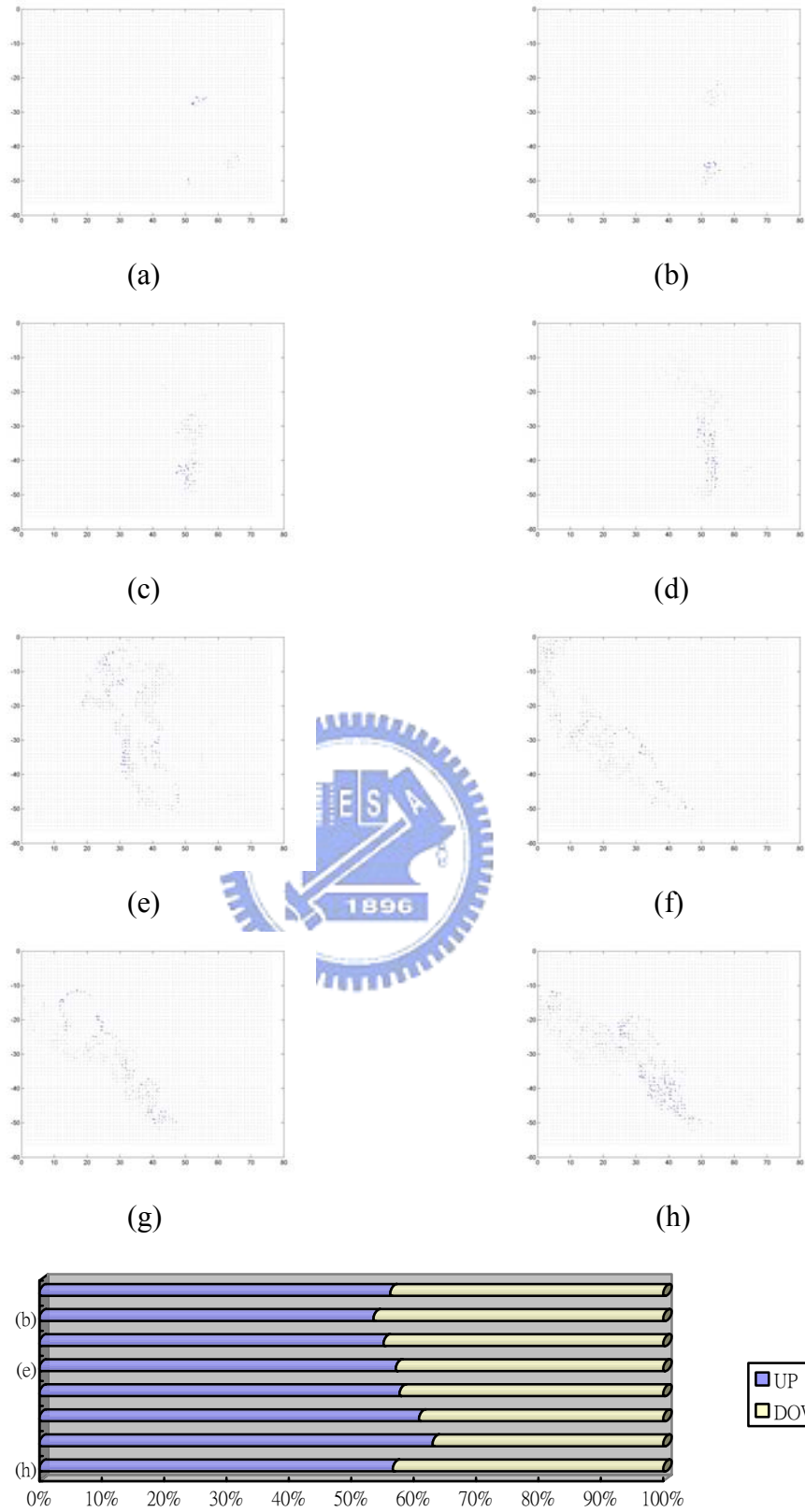


Fig. 4.14. Flow fields applied to Smoke produced on the roadside sequences and the blue part of bar chart shows the percentage of motion upward pixel. Frame number is the same as Fig. 4.13.



(a)



(b)



(c)



(d)



(e)



(f)



(g)



(h)

Fig. 4.15. People walk on the roadside. (a) Frame 50. (b) Frame 100. (c) Frame 150. (d) Frame 200. (e) Frame 250. (f) Frame 300. (g) Frame 350. (h) Frame 450.

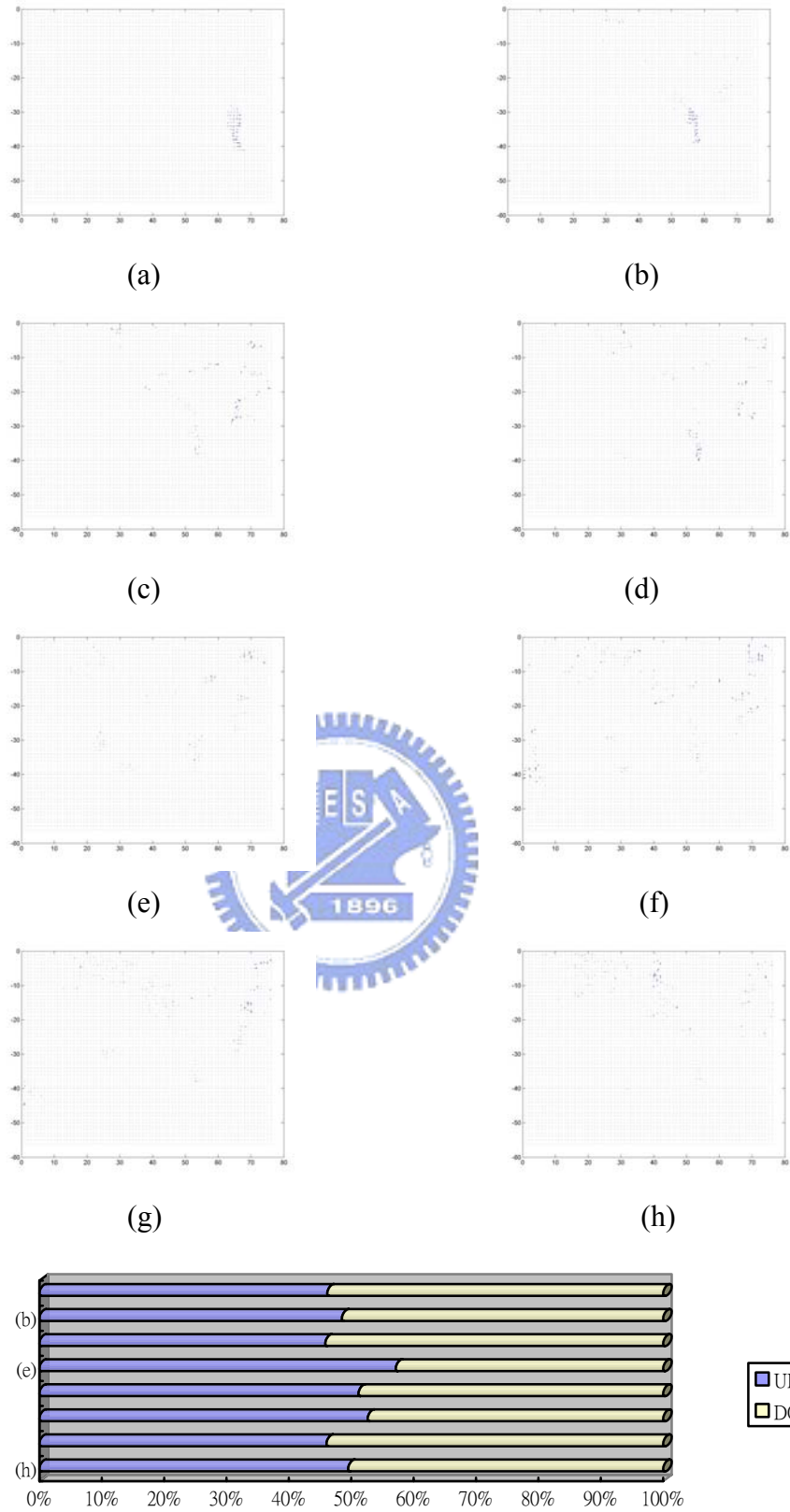


Fig. 4.16. The optical flow fields of moving object internal and the bar chart shows the percentage of motion upward pixel. Frame number is the same as Fig. 4.15.

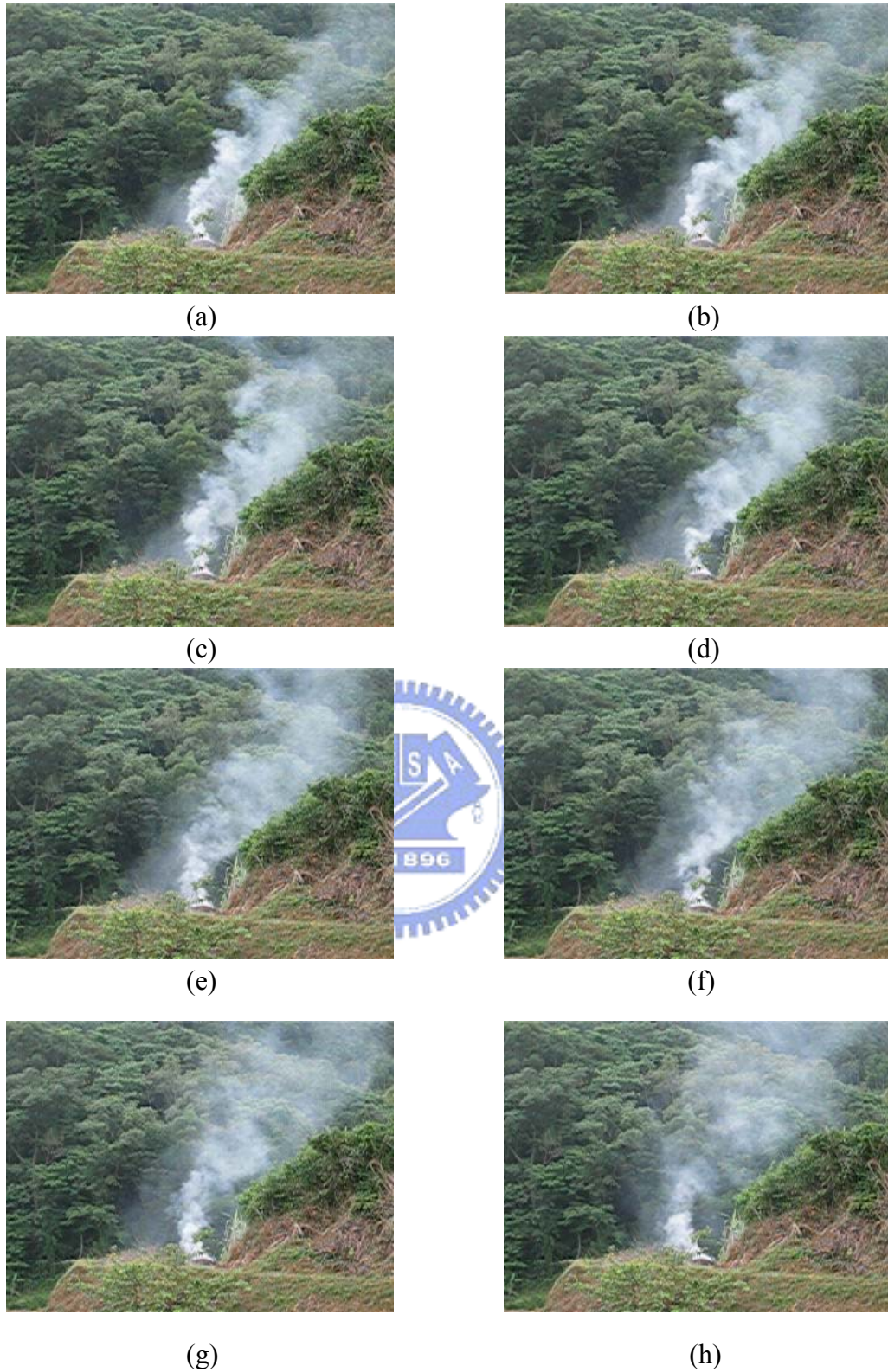


Fig. 4.17. People burn dried straw on the countryside. (a) Frame 50. (b) Frame 100. (c) Frame 150. (d) Frame 200. (e) Frame 250. (f) Frame 300. (g) Frame 350. (h) Frame 450.

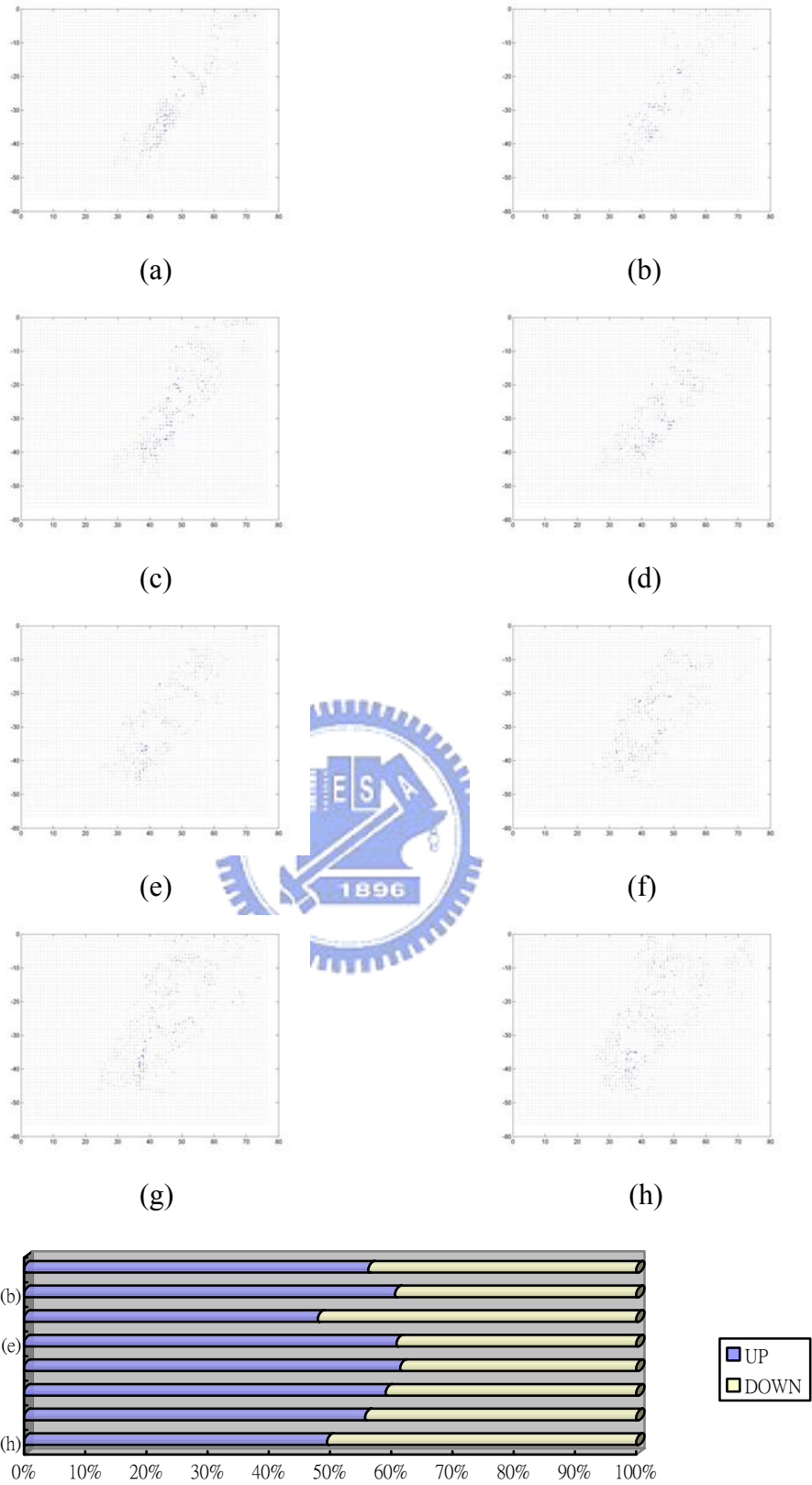


Fig. 4.18. Flow fields applied to Smoke produced while burning dried straw sequences and the blue part of bar chart shows the percentage of motion upward pixel. Frame number is the same as Fig. 4.17.

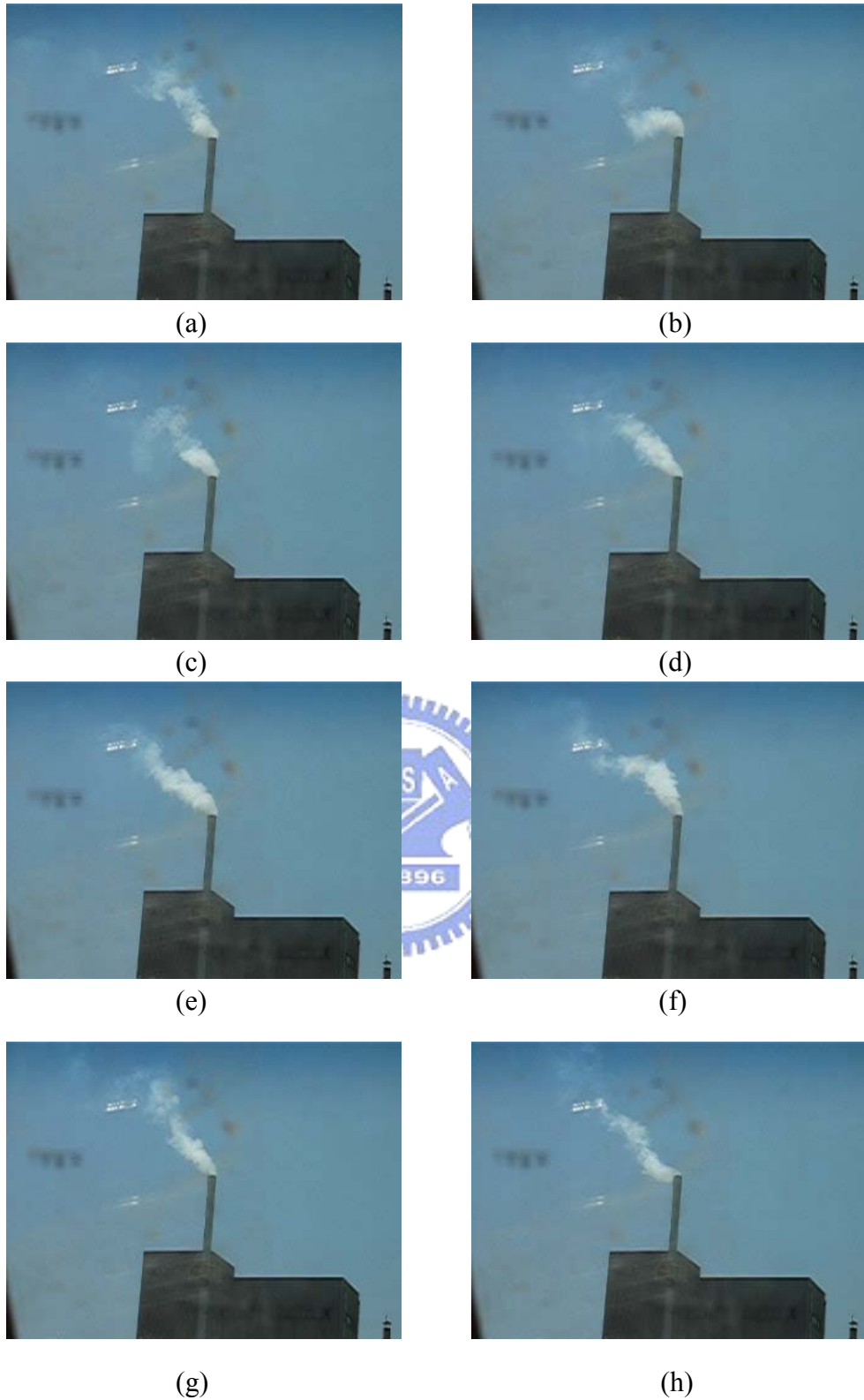


Fig. 4.19. Smoke which is discharged by chimney. (a) Frame 50. (b) Frame 100. (c) Frame 150. (d) Frame 200. (e) Frame 250. (f) Frame 300. (g) Frame 350. (h) Frame 450.

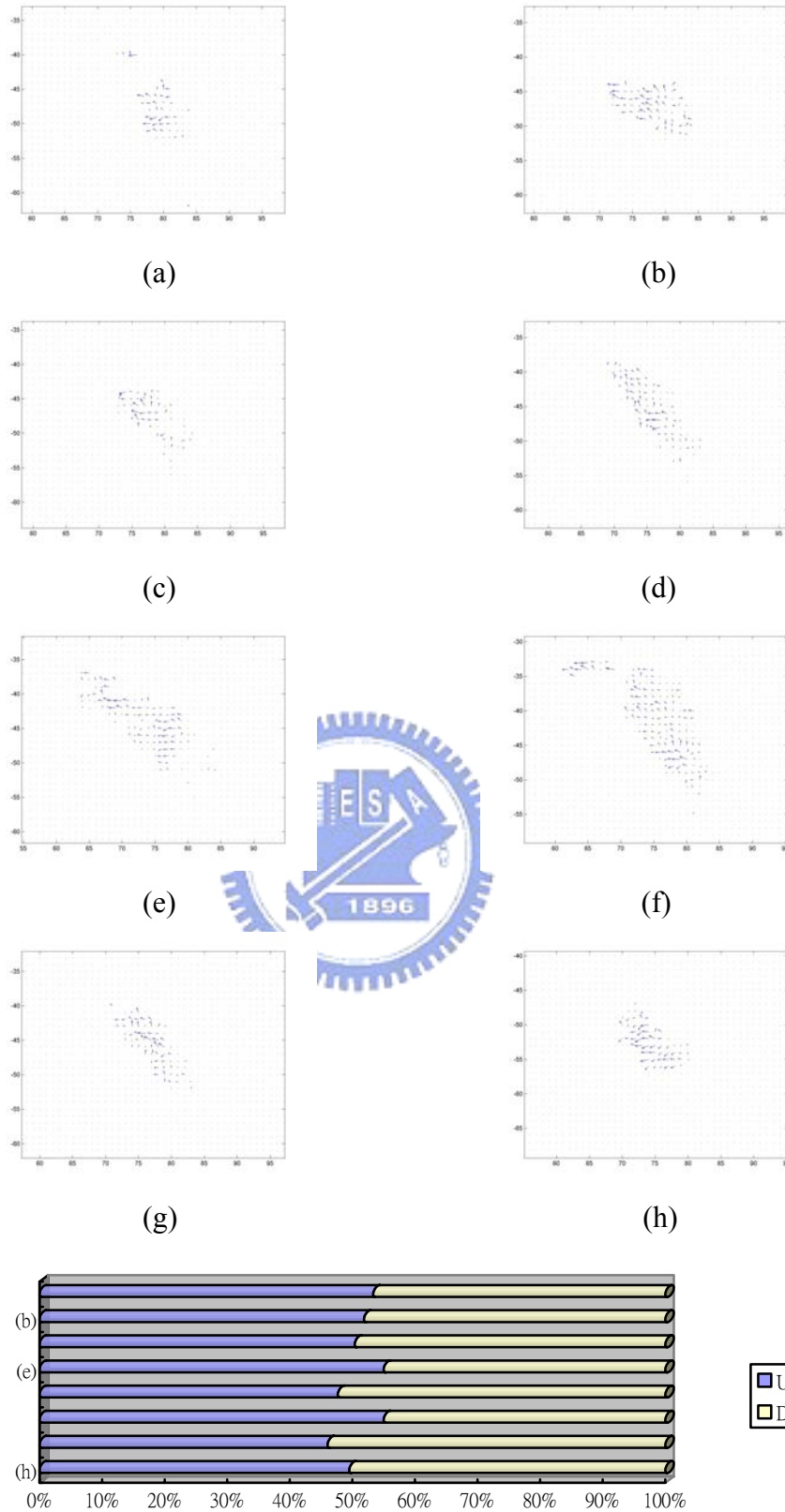


Fig. 4.20. Enlarged optical flow fields of moving object internal and the bar chart still shows the percentage of motion upward pixel. Frame number is the same as Fig. 4.19.

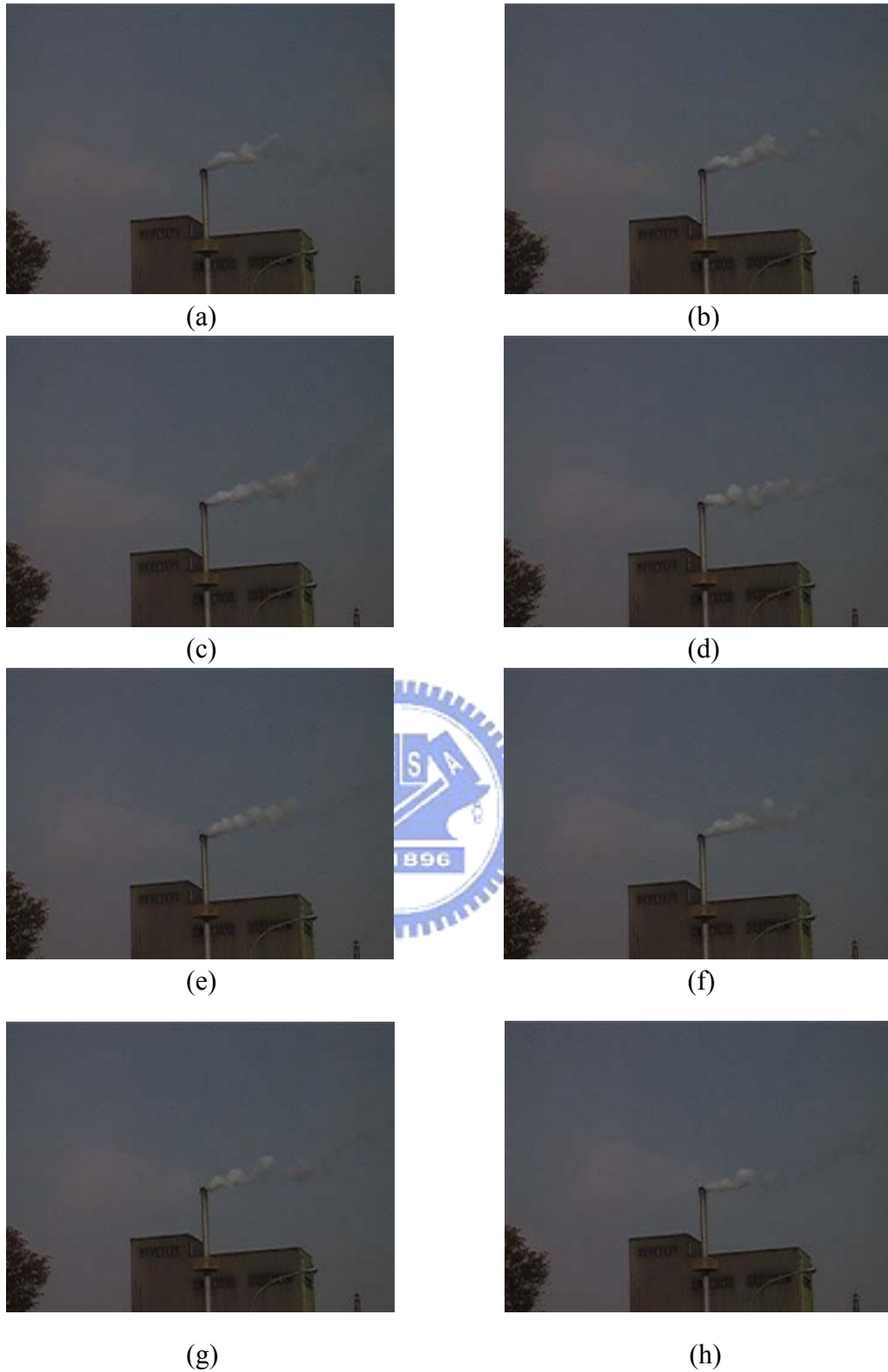


Fig. 4.21. Smoke which is discharged by chimney in strong wind situation. (a) Frame 50. (b) Frame 100. (c) Frame 150. (d) Frame 200. (e) Frame 250. (f) Frame 300. (g) Frame 350. (h) Frame 450.

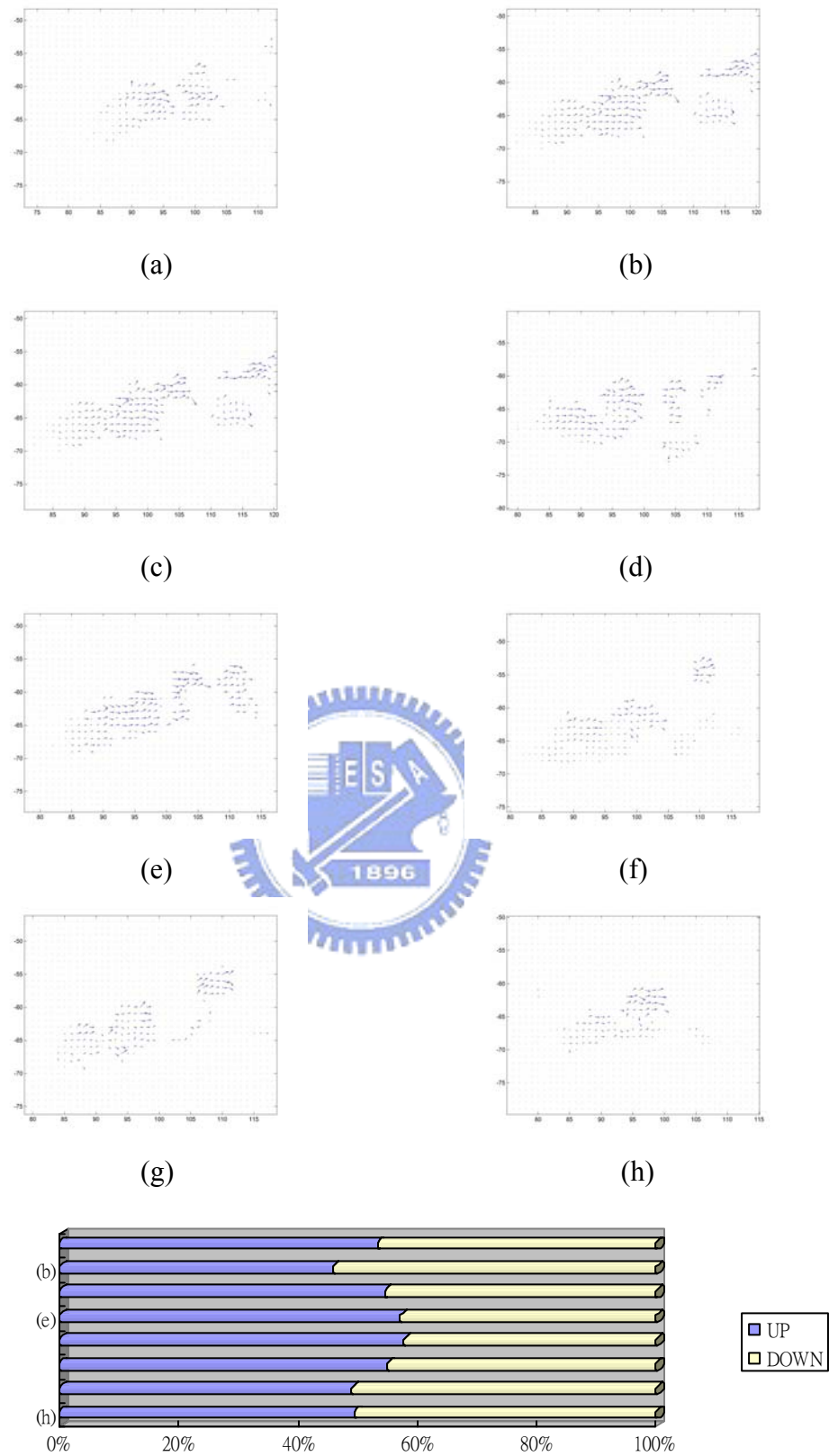


Fig. 4.22. Enlarged optical flow fields of moving object internal and the bar chart still shows the percentage of motion upward pixel. Frame number is the same as Fig. 4.21.

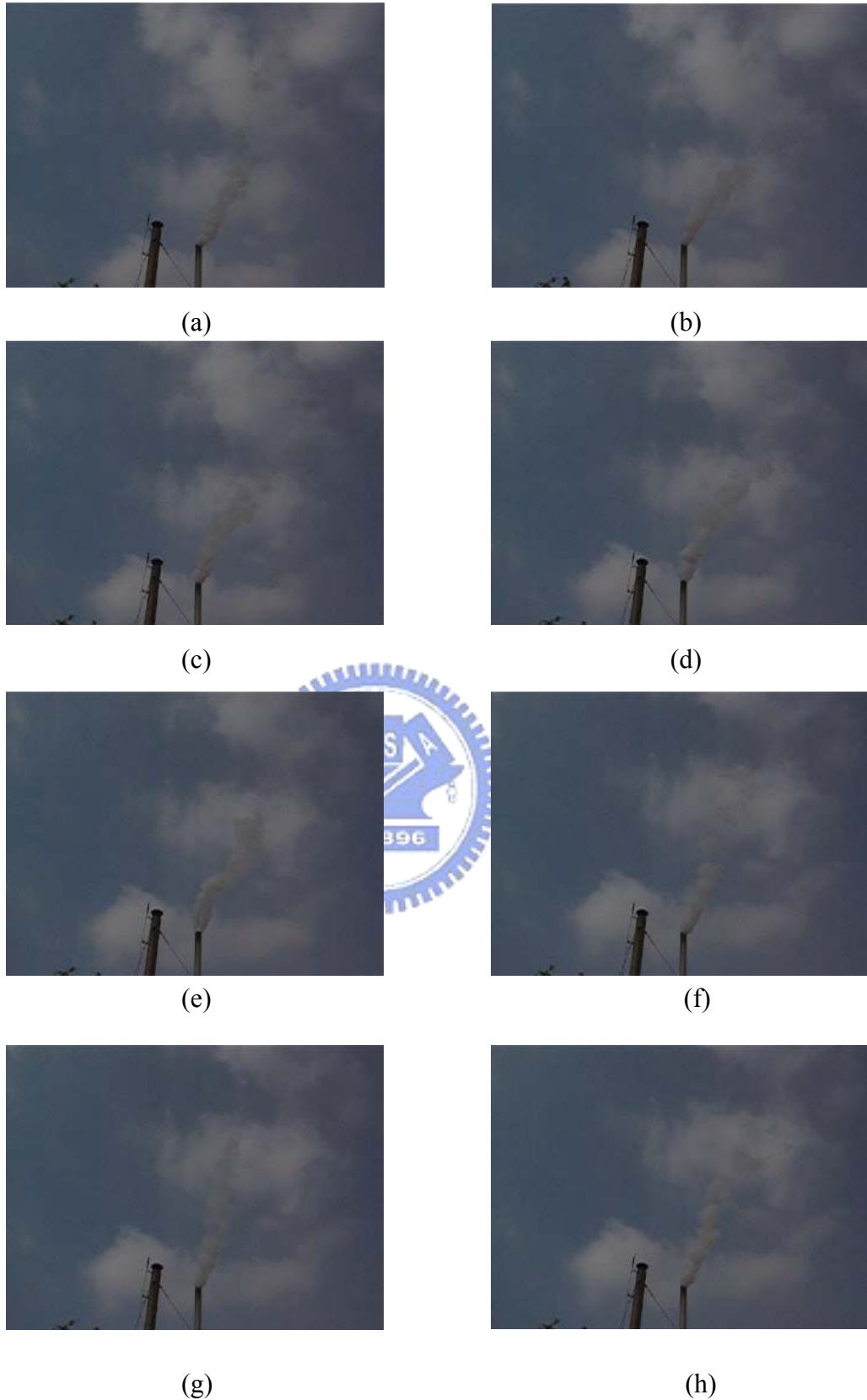


Fig. 4.23. Smoke which is discharged by chimney in strong wind situation and motion of cloud is similar as smoke. (a) Frame 50. (b) Frame 100. (c) Frame 150. (d) Frame 200. (e) Frame 250. (f) Frame 300. (g) Frame 350. (h) Frame 450.

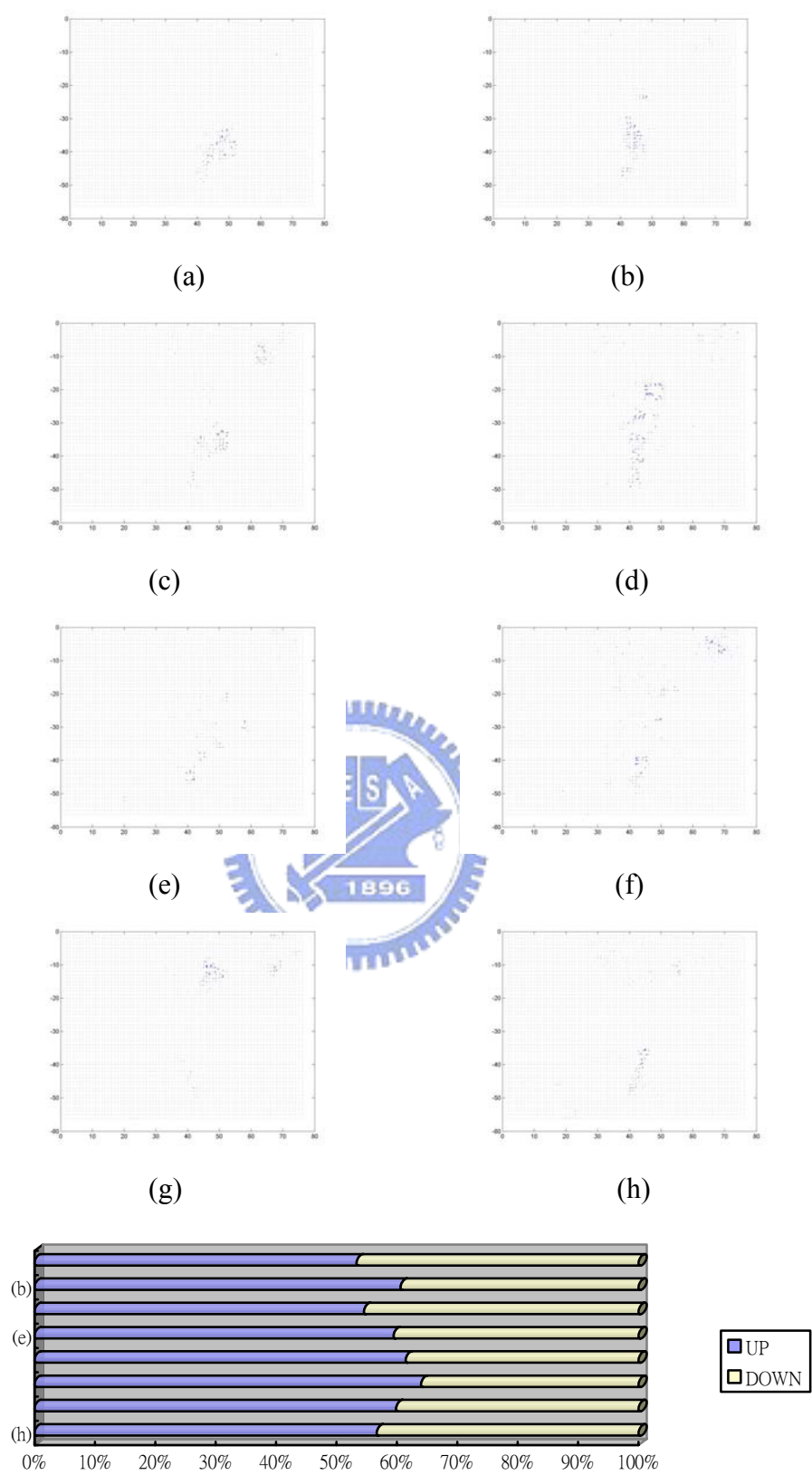


Fig. 4.24. The optical flow fields of moving object internal and the bar chart still shows the percentage of motion upward pixel. Frame number is the same as Fig. 4.23.

4.3 Discussions

In several experiments, we can see the three kinds of degree and defuzzified value in Table. 4.1 and Table. 4.2. We can figure out if the moving object is smoke, the PMUD is larger than 75% generally and if the moving object is not smoke, the PMUD distribute over 40% to 60%. No matter what the moving object moves horizontally or vertically, if we can get the area of moving object large enough, PMUD won't be over 75%. Therefore, PMUD is the most important characteristic that can discriminate from other moving objects. PSD depends on motion of moving object. If the moving object moves to the camera, it also makes PSD higher. About PCD, it will depend on background. If the color of background is similar to moving object, we can't get the whole part of moving object so that PCD is lower. Generally speaking, if the moving object in the scene is smoke, PMUD must be over 75%. Then according to PSD and PCD, we can make sure the moving object is smoke. Although there are many situations that PSD and PCD might be high enough, PMUD is still under 70%. Hence, we can distinguish between smoke and other moving objects. If the area of moving object is not big enough, it will cause the serious erroneous judgement. In Fig. 4.9, the smoke area is not large and the PMUD is not high enough obviously.

Moreover, PMUD is the most important characteristic of smoke. We discuss with it especially. From Table. 4.3 we can know PMUD of smoke will be influenced by wind and if the smoke area in the scene is smaller, in the same situation, PMUD will also be smaller. In the strong wind situation, the motion upward of smoke will be influenced but it still high enough to discriminate from other moving object. If the smoke area in the scene is small, the internal information can't be obtained enough so that it will cause the motion upward of

smoke is not obvious.

Table. 4.3. The PMUD value in different response time.

	30 seconds	45 seconds	60 seconds
PMUD value in first experiment(indoor)	91.43 %	92.56 %	91.89 %
PMUD value in fourth experiment(indoor)	77.56 %	78.32 %	79.88 %
PMUD value in sixth experiment(indoor)	78.46 %	78.89 %	75.23 %
PMUD value in first experiment(outdoor)	92.22 %	93.24 %	93.46 %
PMUD value in third experiment(outdoor)	92.56 %	94.37 %	94.78 %
PMUD value in fourth experiment(outdoor)	88.43 %	88.78 %	87.78 %
PMUD value in fifth experiment(outdoor)	77.43 %	75.42 %	75.25 %

In conclusion, if the visibility of smoke is good enough without wind force, system can detect smoke successfully. When the quantity of smoke is not enough or the background color is similar as smoke color, the visibility of smoke will be quite bad. About outdoor environment, although wind force will influence the motion of smoke, smoke still moves upward continuously and the visibility of smoke is better than indoor environment generally.

Chapter 5

Conclusions

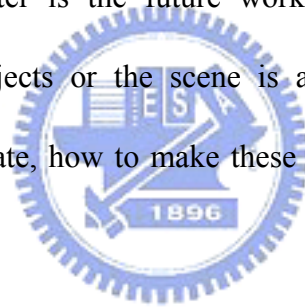
In this thesis, a method for detecting smoke in the fixed scene was proposed. In order to reach the purpose, three features were extracted from dynamic image analysis to represent properties about smoke. Then a fuzzy system was used and the moving object in the scene is smoke or not that is decided according to the output of the fuzzy system.

Although the color characteristic of smoke is not stronger than fire, the motion characteristic of smoke is more obvious. We analyze the smoke and emphasize on motion. The color characteristic of smoke just can help us to discriminate from other moving object which is not gray color. We still depend on the upward movement within the smoke mainly. This is the most important characteristic of smoke. Optical flow method which is proposed by Horn and Schunck, they assume two constraints that fit in smoke. The first constraint is intensity constancy constraint, which states that brightness of an image of any point on the object is invariant under motion. The second constraint is global smoothness constraint, which states in the case neighboring points on the objects have similar velocities and the velocity field of the brightness patterns in the image varies smoothly almost everywhere. In

the experiments, we can know smoke accord with condition very much. It helps us to find the situation within the smoke.

There are many situations that moving objects can get high PSD and PCD but PMUD not. Therefore, the membership function of the PMUD has to set high separating rate. The membership function of PSD and PCD can set low separating rate to get a better toleration. According to the PMUD, we can discriminate between smoke and other moving objects. Then utilize PSD and PCD to increase the correct rate that moving object is smoke.

Image-based smoke detection is still a new field in image processing. How to make these applications of machine intelligence more humanity, doing the right reaction that moving object invades of fire disaster is the future work. Moreover, adding the algorithm to distinguish from moving objects or the scene is an important direction. In addition to improve the detection error rate, how to make these detection methods be utilized in broad place is also very important.



Bibliography

- [1] B.C Arrue, A. Ollero and J.R. Martinez De Dios, "An Intelligent System for False Alarm Reduction in Infrared Forest-Fire Detection," *Intelligence System*, vol.15 , no. 3, May/June 2000, pp.64-73.
- [2] S. Noda and K. Ueda, " Fire Detection in Tunnels Using an Image Processing Method," in *proceedings of the 1994 Vehicle Navigation and Information System Conference* , 1994, pp. 57-62.
- [3] G. Healey, D. Slater, T. Lin, B. Drda and A.D. Goedeke, "A System for Real-time Fire Detection," In *Proceedings of the IEEE Conference on Computer Vision and Pattern Recognition*, 1994, pp. 605-606.
- [4] S.Y. Foo, "A Machine Vision Approach to Detect and Categorize Hydrocarbon Fires in Aircraft Dry Bays and Engine Compartments," *IEEE Transactions on Industry Applications*, vol. 36, no. 2, March/April 2000, pp. 459-466.
- [5] Wen-Bing Horng and Jian-Wen Peng, "Real-time Fire Detection from Video: A Preliminary Report," *Proc. of the 14th IPPR Conference on Computer Vision Graphics and Image Processing*, Taipei, 2001.

- [6] W. Phillips III, M. Shah and N. da Vitoria Lobo, "Flame Recognition in Video," in *Proceeding of the Fifth IEEE Workshop on Applications of Computer Vision*, 2000, pp.224-229.
- [7] V. Capellini, L. Mattii and A. Mecocci "An intelligent system for automatic fire detection," *IEEE Third International Conference on Image Processing and its Applications*, 1989.
- [8] Philippe Guillemant and Jérôme Vicente, "Real-time identification of smoke images by clustering motions on a fractal curve with a temporal embedding method," in *Society of photo-optical instrumentation Engineers*, vol. 40 no. 4, April 2001.
- [9] R.C. Gonzalez and R.E. Woods, *Digital Image Processing*, Reading, MA: Addison Wesley, 1993.
- [10] C.T. Lin and C.S. G. Lee, *Neural Fuzzy System*, Reading, MA: Prentice-Hall Publishing, 1999.
- [11] B.K.P. Horn and B. Schunck, "Determining Optical Flow," *Artificial Intelligence*, vol. 17, no. 572, pp. 185-203, Apr. 1981.
- [12] B. Lucas and T. Kanade, "Performance of Optical Flow Techniques," *Proc. Image Understanding Workshop*, pp. 121-130, July 1981.
- [13] H.H. Nagel, "On the Estimation of Optical Flow: Relation between Different Approaches," *Artificial Intelligence*, vol. 33, no. 3, pp. 299-324, June 1987.
- [14] S. Ghosal and R. Mehrotra, "Robust Optical Flow Estimation," *Proc. IEEE Int'l Conf. Image Processing*, vol. 2, pp. 780-784, Aug. 1994.
- [15] R. Li, B. Zeng and M.L. Liou, "A New Three-Step Search Algorithm for Block Motion Estimation," *IEEE Trans. Circuits and Systems for Video Technology*, vol. 4, no. 4, pp.



438-442, Aug. 1994.

- [16] X. Xia and Y.Q. Shi, "A Thresholding Hierarchical Block Matching Algorithm for Motion Estimation," *IEEE Int'l Symp. Circuits and Systems*, vol. 2, pp. 624-627, May 1996.
- [17] M.J. Chen, L.G. Chen and T.D. Chiueh, "One-Dimensional Full Search Motion Estimation Algorithm for Video Coding," *IEEE Trans. Circuits and Systems for Video Technology*, vol. 4, no. 5, pp. 504-509, Oct. 1994.
- [18] G. Gupta and C. Chakrabarti, "Architectures for Hierarchical and Other Block Matching Algorithms," *IEEE Trans. Circuits and Systems for Video Technology*, vol. 5, no. 6, pp. 477-489, Dec. 1995.
- [19] D.J. Heeger, "Optical Flow using Spatiotemporal Filters," *Int'l J. Computer Vision*, vol. 1, no. 4, pp. 279-302, Jan. 1988.
- [20] J.L. Barron, D.J. Fleet and S.S. Beauchemin, "Performance of Optical Flow Techniques," *Int'l J. Computer Vision*, vol. 12, no. 1, pp. 43-77, Feb. 1994.
- [21] N. Otsu, "A threshold selection method from gray-level histogram," *IEEE Trans. on System, Man and Cybernetics*, vol. 9, no. 1, pp. 62-66, January, 1979.